A single-parasite transcriptional atlas of *Toxoplasma gondii* reveals novel control of antigen expression

Yuan Xue[1], Terence C. Theisen[2], Suchita Rastogi[2], Abel Ferrel[2], Stephen R. Quake[1,3,4,*], John C. Boothroyd[2,*]

[1]Department of Bioengineering, [3]Department of Applied Physics, Stanford University, Stanford, CA, USA
[2]Department of Microbiology and Immunology, Stanford University School of Medicine, Stanford, CA, USA
[4]Chan Zuckerberg Biohub, San Francisco, CA, USA
*Correspondence should be addressed to J.C.B. (jboothr@stanford.edu) and S.R.Q. (steve@quake-lab.org)

Abstract

Toxoplasma gondii, a protozoan parasite, undergoes a complex and poorly understood developmental process that is critical for establishing a chronic infection in its intermediate hosts. Here, we applied single-cell RNA-sequencing (scRNA-seq) on >5,400 Toxoplasma in both tachyzoite and bradyzoite stages using three widely studied strains to construct a comprehensive atlas of cell-cycle and asexual development, revealing hidden states and transcriptional factors associated with each developmental stage. Analysis of SAG1-related sequence (SRS) antigenic repertoire reveals a highly heterogeneous, sporadic expression pattern unexplained by measurement noise, cell cycle, or asexual development. Furthermore, we identified AP2IX-1 as a transcription factor that controls the switching from the ubiquitous SAG1 to rare surface antigens not previously observed in tachyzoites. In addition, comparative analysis between *Toxoplasma* and *Plasmodium* scRNA-seq results reveals concerted expression of gene sets, despite fundamental differences in cell division. Lastly, we built an interactive data-browser for visualization of our atlas resource.

Keywords: single-cell RNA sequencing, protozoa, cell cycle, *Toxoplasma*, development, AP2 transcription factor

Main text

Introduction

Toxoplasma gondii is an intracellular protozoan parasite that is thought to infect over a quarter of the world's population[1]. Like some of its *Apicomplexan* cousins, *Toxoplasma* undergoes a complex developmental transition inside the host. In intermediate hosts, including humans and virtually all other non-feline, warm-blooded animals, *Toxoplasma* parasites remain haploid and transition from a replicative, virulent tachyzoite to an encysted, quasi-dormant bradyzoite. This asexual developmental transition is tightly coupled to the clinical progression of *Toxoplasma* infection. Although acute infection with tachyzoites produces few if any symptoms in healthy human children and adults, infected individuals, if left untreated, progress to a chronic stage wherein tachyzoites transition to bradyzoites that can persist for life in neurons and muscle cells. When infected individuals become immunocompromised, such as in chemotherapy, HIV infection, or organ transplantation[2,3], bradyzoites can reactivate to become tachyzoites, causing severe neurological damage and even death. While no causal link has been established, a population-wide study has uncovered significant association of *Toxoplasma* infection with schizophrenia in chronically infected humans[4]. Chronic infection in mice has been observed to induce behavioral changes such as loss of aversion to cat urine, which is hypothesized to increase the transmission rate of *Toxoplasma* to its definitive feline host where sexual reproduction occurs[5]. As there are no therapeutic interventions to prevent or clear cysts in infected individuals, understanding how *Toxoplasma* transitions through its life stages remains of critical importance.

The development of *in vitro* methods to induce *Toxoplasma* differentiation have facilitated investigation of several aspects of chronic infection, including transition of tachyzoites to bradyzoites[6,7]. Bulk transcriptomic analyses of *Toxoplasma gondii* at distinct asexual stages reveal genetic modules that are expressed in each stage[8–15], including AP2 transcription factors that are thought to play a role in differentiation[16,17]; however, transitioning parasites convert to the bradyzoite stage asynchronously and display a high degree of heterogeneity along the developmental pathway and in gene expression[18,19]. Furthermore, parasites within the same tissue cysts have been shown to display heterogeneity in the expression of bradyzoite marker proteins[20]. The transition of tachyzoites to the bradyzoite stage results in an overwhelming majority of mature bradyzoites in the G_1 phase of the cell cycle that divide slowly, if at all[21,22]. Furthermore, tachyzoites exhibit slower growth kinetics immediately prior to the bradyzoite transition[21,23]. This suggests that parasites exit the cell cycle to differentiate into bradyzoites, a pattern consistent with developmental processes in several other eukaryotic organisms[24,25]. Dissecting these cell cycle aspects of stage conversion

requires a more detailed analysis than has been possible with bulk measurement of tachyzoite or bradyzoite populations, or with the use of genetically modified parasites coupled with chemical synchronization of cell cycle progression[13,26–28]. This is because the latter approaches require large quantities of synchronized parasites and can potentially introduce artificial perturbations. Furthermore, bulk measurement fails to distinguish parasite-to-parasite variation that is independent of cell cycle or known developmental processes, potentially missing the phenotypic diversity intrinsic to a population of cells.

Single-cell RNA sequencing (scRNA-seq) offers a powerful and unbiased approach to reveal the underlying heterogeneity in an asynchronous population of cells. Droplet and FACS-based approaches have already been applied towards multicellular parasites such as *Schistosoma* to reveal developmental changes within different hosts[29]. Recently, scRNA-seq has revealed a surprising degree of heterogeneity in another apicomplexan parasite, *Plasmodium*[30–33]. Analyses derived from these single-parasite measurements uncovered rare and critical transition events in parasite development that were undetectable in bulk measurements. Combined with novel analytical tools and increase in measurement throughput, scRNA-seq can help facilitate the discovery of regulatory factors that mediate these developmental transitions in a system-wide fashion.

Here, we performed scRNA-seq to reconstruct transcriptional dynamics of asynchronous *Toxoplasma* parasites in the course of cell cycle and asexual development *in vitro*. Our analysis reveals the existence of hidden cell states and rare parasites that show highly unusual patterns of gene expression associated with specific transcription factors. We also discover that individual parasites vary substantially in the expression of surface antigen genes, suggesting the possibility of a novel form of antigenic variation that may play a crucial role in host immunity evasion. Importantly, we identified a single parasite from our scRNA-seq dataset that displayed an unusual expression pattern of surface antigens, leading us to identify and validate the regulatory role of a previously uncharacterized AP2 transcription factor typically associated with parasites in sexual development. Lastly, we show that despite fundamental differences in their modes of cell division, there are conserved transcriptional programs between the asexual life cycles of *Toxoplasma gondii* and *Plasmodium berghei*. Our results combined provide the first comprehensive single-cell atlas of *Toxoplasma* in the course of asexual development and help reveal that the antigenic repertoire of this parasite is much more heterogeneous than previously appreciated.

Results

Technical validation of single-parasite sorting and sequencing

There are more than a dozen approaches available for single-cell isolation and transcriptome amplification. Based on benchmark comparisons, Smart-seq2 generally has higher sensitivity than competing droplet-based approaches[34,35]. We reasoned that sensitive measurement is crucial in our study, given that single *Toxoplasma gondii* parasites are at least 50-fold smaller in volume than a typical mammalian cell, and thus the average parasite gene is likely expressed with much lower copy number per cell than a typical mammalian gene. For our initial studies, we used the common Type I lab strain of *Toxoplasma*, RH, grown *in vitro* in human foreskin fibroblasts (HFFs). Following such growth, individual tachyzoites were released by passage through a narrow-gauge needle and then purified by fluorescence activated cell sorting (FACS) into 384-well or 96-well plates. We then synthesized, amplified, and barcoded cDNA using Smart-seq2 and Illumina Nextera protocols. We reduced the reagent cost in 384-well plates effectively by ten-fold compared to the 96-well format. The sequenced reads were bioinformatically deconvolved and grouped into individual parasites for analysis using modified bcl2fastq and custom python scripts (**Materials and methods**). A schematic to illustrate our experimental workflow is shown in **Figure 1**.

To ensure that our workflow efficiently captures single *Toxoplasma* parasites, we mixed equal numbers of two transgenic lines of RH, one expressing GFP and the other expressing mCherry, and sorted individual parasites into a 384 well plate based on the presence of either green or red fluorescence. After Smart-seq2 amplification, we quantified the expression of GFP and mCherry mRNAs using quantitative polymerase chain reaction (qPCR). Across all 301 wells that we measured, we observed the presence of both GFP and mCherry mRNA in only one well, indicating that the rate of doublet events is below 1% (**Figure 1 - Supplementary Figure 1a**). To address the possibility that the reduced reagent volume in the 384-well format could potentially saturate the reaction chemistry and thus limit quantification range, we sorted varying numbers of RH and quantified with qPCR the mRNA of a gene encoding the abundantly expressed surface protein, SRS29B (SAG1) (**Figure 1 - Supplementary Figure 1b**). The detected amount of SAG1 mRNA present in wells containing single, eight, or fifty RH fell into the expected distributions based on the number of parasites sorted, without signs of saturation, indicating that the assay is capable of quantitative measurement at the single *Toxoplasma* level. We then proceeded to sort parasites into 384-well based on live/dead staining and sequence 729 RH (612 passed quality control) strain single *Toxoplasma* parasites from asynchronous populations grown under tachyzoite conditions. We also sorted and sequenced 287 RH parasites (237 passed quality control) into 96-well plate for comparison, which we will discuss further in another

142section. For Pru and ME49 strains, we collected parasites at several time points post
143alkaline treatment which induces differentiation from tachyzoites to bradyzoites to follow
144changes in their expression profiles during *in vitro* development (**Materials and**
145**methods**), yielding 2655 Pru (2198 passed quality control) and 1828 ME49 (1552
146passed quality control) single parasites. RH reads were aligned to the GT1 strain
147genome, which is the most complete reference for Type I parasites, while Pru and ME49
148were aligned to the ME49 strain Type II genome reference. Because many genes
149encoding *Toxoplasma* secretion factors and surface proteins are evolutionary products
150of gene duplication events[36], we expected high sequence similarity amongst a
151substantial portion of the parasite genes. Thus, we modified our gene counting pipeline
152to account for duplicated genes by distributing reads across all regions with equal
153alignment score that passed thresholds (**Materials and methods**). The reason why we
154adopted a correction scheme for multiply-mapped reads is because the analysis of co-
155occurrence, or lack thereof, of pathogenic factors (e.g. surface antigens) hinges on
156sensitive detection of their expression. We thus faced a choice of increasing the false
157positive in gene alignment by correcting for multiply mapped reads or increasing its
158false negative by counting only uniquely aligned reads. We chose to account for multiply
159mapped genes, which would otherwise be obscured, as we hypothesized that surface
160antigen expression may vary between individual parasites, which we further discuss in
161another section. A comparison of counting methods does not reveal significant
162differences in the observed counts (**Figure 1 - Supplementary Figure 1c**). Further
163analysis reveals that our modified pipeline recovered the detection of more parasite
164genes than default parameters (**Figure 1 - Supplementary Figure 1d**).
165 To ensure that poorly amplified or sequenced parasites did not confound our
166downstream analysis, we filtered samples based on several quality metrics including
167percent reads mapping to ERCC spike-in sequences, number of genes detected, and
168sequencing depth (**Materials and methods**; **Figure 1 - Supplementary Figure 2a**). On
169average, each sequenced parasite contains 30-50% reads that mapped to *Toxoplasma*
170genes encoding proteins (top panel in **Figure 1 - Supplementary Figure 2b**). Most of
171the unmapped reads are from *Toxoplasma*'s 28s ribosomal RNA. The relatively high
172rate of rRNA contamination was also observed in single-parasite RNA sequencing of
173*Plasmodium*[30]. We suspect this occurred due to non-specific priming as protozoan cells
174have low RNA input. We normalized for sequencing depth across cells by dividing each
175read count by the read sum of each corresponding cell and then multiplied by the
176median of read sum within each dataset to yield "count per median" (CPM). After
177filtering ERCC spike-in and rRNA genes, we detected on average 862, 1290, and 970
178genes per parasite with greater than or equal to 2 read counts (**Materials and**
179**methods**) in the RH, Pru, and ME49 datasets, respectively (bottom panel in **Figure 1 -**
180**Supplementary Figure 2b**). Characterization of our measurement sensitivity based on
181logistic regression modeling of ERCC spike-in standards (**Materials and methods**)[37]
182reveals a 50% detection rate of 17, 17, and 26 molecules for RH, Pru, and ME49

183datasets, respectively (top panels in **Figure 1 - Supplementary Figure 2c**). The
184sensitivity of our 384-well Smart-seq2 measurement is comparable to the previously
185reported range for the 96-well format[38]. As expected from our qPCR titration experiment,
186scRNA-seq measurement of gene expression is quantitative at single parasite
187resolution based on ERCC standards. We determined that the linear dynamic range of
188our scRNA-seq measurement spans over three orders of magnitude (bottom panels in
189**Figure 1 - Supplementary Figure 2c**). Taken together, we demonstrate a scalable and
190cost-effective approach to measure the transcriptomic changes of individual parasites
191with high sensitivity and accuracy.

192**Cell cycle landscape of asynchronous *Toxoplasma***

193 Previous work posited a potential link between bradyzoite development and cell
194cycle, which poses a significant challenge to the bioinformatic analysis of either
195process[21]. To characterize cell cycling changes without confounding contributions from
196developmental processes, we first analyzed an asynchronous population of Type I RH
197strain parasites grown under tachyzoite conditions; this extensively passaged lab strain
198is known to have little propensity to switch to bradyzoites under such conditions[6]
199(**Materials and methods**). After filtering out genes whose expression levels did not vary
200significantly between individual parasites, we projected the data with principal
201component analysis (PCA) (**Materials and methods**). Interestingly, the first two
202principal components (PCs) reveal a circular trajectory that coincides with relative DNA
203content, determined using a cell permeable DNA content stain (top panel in **Figure 2a**).
204Unsupervised neighborhood clustering identified five distinct clusters of parasites based
205on their transcriptional profiles (middle panel in **Figure 2a**) (**Materials and methods**).
206We computed RNA velocity to infer transcriptional dynamics[39,40] and the velocity vector
207field indicates a net “counter-clockwise” flow of transcriptional changes (bottom panel in
208**Figure 2a**) (**Materials and methods**). We assigned cell cycle phase to the clusters
209based primarily on change in DNA content (**Figure 2 - Supplementary Figure 3a**) but
210also considering previous bulk transcriptomic characterization[28] (**Figure 2 -**
211**Supplementary Figure 3b**). Unsupervised clustering identified two distinct clusters in
212G_1 state, which we have designated as G_1a and G_1b. We found a list of differentially
213expressed genes between the two G_1 clusters. The G_1a cluster is highly enriched for the
214expression of metabolic genes such as phenylalanine hydroxylase (*TGGT1_411100*)
215and pyrroline-5-carboxylate reductase (*TGGT1_236070*), as well as invasion-related
216secreted factors such as MIC2 (*TGGT1_201780*), MIC3 (*TGGT1_319560*), and MIC11
217(*TGGT1_204530*). On the other hand, G_1b cluster is enriched for the expression of 3-
218ketoacyl reductase (*TGGT1_217740*) and cytidine and deoxycytidylate deaminase
219(*TGGT1_200430*), as well as numerous uncharacterized proteins (**Supplementary File**
220**2**). The relative abundance of G_1a, G_1b, S, M, and C states were determined to be 18%,
22132%, 28%, 15%, and 7%, respectively. Without chemical synchronization, the

222correlation between the scRNA-seq data of asynchronous parasites and previously
223published bulk transcriptomic measurement suggests strong agreement in cluster
224assignment and cell cycle state identification (**Figure 2 - Supplementary Figure 3b**).
225This highlights a key advantage of scRNA-seq, as it enables identification of cell cycle
226status of a parasite without reliance on chemical induction, which may lead to unnatural
227cellular behavior.
228 To verify the cyclical nature of gene expression through the lytic cycle, we
229reconstructed a biological pseudotime of RH using Monocle 2 (**Materials and**
230**methods**). The results show a clear oscillatory expression pattern for the variably
231expressed genes along the pseudotime axis (**Figure 2b**). To further characterize cell
232cycle expression patterns, we clustered genes based on pseudotime interpolation and
233hierarchical clustering (**Materials and methods)**. Some of the key organelles in
234tachyzoites are made at different times in the cell cycle[28]. To confirm and refine this
235finding, we calculated the mean expression values for each set of organelle-specific
236genes based on their annotation in ToxoDB[41] (**Supplementary File 4**). This showed the
237expected, strong oscillation with pseudotime (bottom panel in **Figure 2 -**
238**Supplementary Figure 3c**), which also strongly correlates with the oscillation of DNA
239and total mRNA content (top panels in **Figure 2 - Supplementary Figure 3c**). On the
240other hand, we also observed instances where a given gene's expression was
241discordant to the dominant trend of its nominal organelle set (arrows in **Figure 2 -**
242**Supplementary Figure 3d**). For example, 63.5% of genes annotated as rhoptry (ROP)
243or rhoptry neck (RON) are assigned pseudotime cluster 3, while the remaining 36.5%
244rhoptry genes are assigned pseudotime clusters 1 or 2 (**Figure 2 - Supplementary**
245**Figure 3e**). Specifically, genes annotated as ROP33 and ROP34, based on their
246homology to genes encoding known rhoptry proteins, are assigned to cluster 2 instead
247of cluster 3 (left panel in **Figure 2 - Supplementary Figure 3f**). Recent reports have
248experimentally determined these two to be non-rhoptry-localizing proteins. This is
249consistent with our observation of discordance between their and known ROPs'
250expression profiles along the pseudotime[42]. Through analysis of pseudotime clustering,
251we also identified genes not annotated as ROPs within the ROP-dominated cluster 3,
252such as *TGGT1_218270* and *TGGT1_230350*, that have recently been shown to
253encode *bona fide* rhoptry and rhoptry neck proteins, now designated as ROP48 and
254RON11, respectively[43,44] (left panel in **Figure 2 - Supplementary Figure 3f**). As another
255example, IMC2a peaks in expression level in G_1, while the majority of inner-membrane
256complex (IMC) genes are expressed towards the M/C phase of the cell cycle (right
257panel in **Figure 2 - Supplementary Figure 3f**). A recent report has proposed
258reannotation of IMC2a as a dense granule (GRA) protein (GRA44) based on subcellular
259localization[45], which is consistent with our unsupervised group assignment of IMC2a as
260falling in cluster 1 where GRA genes dominate. A list of 8590 RH genes with their
261corresponding pseudotime clustering assignment is provided (**Supplementary File 5**).
262We observe high discordance of pseudotime expression for several genes in each

263annotated organelle sets, suggesting that the current *Toxoplasma* annotation may need
264significant revision. Our scRNA-seq data provide an important resource to help identify
265mis-annotated genes and infer putative functions of uncharacterized proteins.

266**Hidden heterogeneity in asexually developing *Toxoplasma***

267 *Toxoplasma* has one of the most complicated developmental programs of any
268single-celled organism; however, it is unknown how synchronized the transition is
269between developmental states. To address this, we assessed the inherent
270heterogeneity within asexually developing Pru, a type II strain that is capable of forming
271tissue cysts with characteristics that resemble early "bradyzoites" from *in vivo* source
272upon growth in *in vitro* alkaline conditions[18,46]. We applied scRNA-seq to measure and
273analyze Pru parasites grown in HFFs as tachyzoites ("uninduced") and after inducing
274the switch to bradyzoites by growth in alkaline media for 3, 5, and 7 days. Projection of
275the first two PCs of uninduced Pru tachyzoites (Day 0) reveals the expected circular
276projection (**Figure 3 - Supplementary Figure 4a**), presumably reflecting cell cycle
277progression as seen for the RH tachyzoites, described above. To validate this, we
278developed a random forest classifier model based on our cell cycle assignment in RH
279(**Materials and methods**). Comparable to what we observed in RH, cell cycle prediction
280reveals that the uninduced population of Pru is composed of 28%, 41%, 21%, 7%, and
2813% parasites in G_1a, G_1b, S, M, and C states, respectively. Consistent with previous
282observation[23], our data show most induced Pru parasites (Day 3 - 7) are in the G_1 state
283with a predominance of G_1b (**Figure 3 - Supplementary Figure 4b**).
284 To identify transcriptomic changes associated with the tachyzoite-bradyzoite
285transition, we next projected data from both induced and uninduced Pru parasites onto
286two dimensions using UMAP, a nonlinear dimensionality reduction method (**Materials**
287**and methods**)[47]. Unsupervised clustering revealed six distinct clusters of parasites,
288which we label P1-6 (**Figure 3a**). Cluster formations partially correlate with treatment
289time points and cell cycle states (**Figure 3b; Figure 3 - Supplementary Figure 4c**),
290suggesting that the asexual differentiation program overlaps with cell cycle regulation in
291*Toxoplasma,* as proposed previously[21]. We stratified the datasets by days post alkaline
292induction (dpi) and observed elevated expression of previously described "early"
293bradyzoite marker genes in induced parasites, including *SRS44* (*CST1*) and *BAG1*, with
294a concomitant reduction in expression of *SRS29B (SAG1)*, a tachyzoite-specific surface
295marker gene (**Figure 3 - Supplementary Figure 5**). The abundance of $SAG1^+$ parasites
296(72%) in the induced population suggests two possible interpretations: (1) the depletion
297of SAG1 mRNA is relatively slow and we are measuring SAG1 transcripts made when
298the parasites were still tachyzoites, or (2) the asexual transition induced by alkaline
299treatment is highly asynchronous. Interestingly, RNA velocity analysis suggests that P3
300may be a fate decision point as the trajectory trifurcates into either P4 (cell cycle), P1, or

301P2 as evident by the net transcriptional flow (compare **Figure 3a** to right panel in **Figure**
302**3b**).
303 To determine the gene modules specific to a given cluster, we conducted
304differential gene expression for each cluster (**Figure 3c** and **Supplementary File**). P1
305cluster cells are enriched for expression of bradyzoite-specific genes while P2-5 are
306enriched for that of tachyzoite-specific or cell cycle-associated genes (**Figure 3c-d**). In
307our scRNA-seq data, we also observe a small portion of *BAG1*$^{+}$ bradyzoites (7.1%)
308annotated as either S, M, or C states, indicating that they are replicating (**Figure 3 -**
309**Supplementary Figure 4d**). Our data supports the notion that bradyzoites can undergo
310cell cycle progression[19]. We observe a family of transcription factors known as Apetala 2
311(AP2) that are differentially expressed across different clusters, some of which are
312implicated in *Toxoplasma* development[48–50] (**Figure 3e**). In particular, we identify AP2Ib-
3131, AP2IX-1, AP2IX-6, and AP2VI-2 as over-expressed in P1, suggesting their potential
314roles in the regulation of developmental transition, while AP2IX-9, AP2X-8, AP2VIIa-6,
315AP2XI-1, AP2IX-3, AP2VIII-7, and AP2-domain protein TGME49_215895 (not yet
316assigned a formal AP2 number), are highly expressed in P6, hinting at their possible
317roles in defining this distinct cluster of parasites.
318 The most highly expressed genes in P6 include genes enriched in P2 as well as
319bradyzoite-specific genes found in P1 (**Figure 3c**). To identify genes that are specifically
320expressed in P6, we used Wilcoxon's test (**Figure 3 - Supplementary Figure 6a**)
321(**Materials and methods)** between P6 and P2 or P1. Comparison of our data to
322previous bulk transcriptomic measurement in tachyzoites, tissue cyst, or isolates at the
323beginning or the end of sexual cycle showed no specific enrichment in known
324developmental stages (**Figure 3 - Supplementary Figure 6b**)[51]. Instead, we show that
325based on their expression, P6 forms a distinct sub-population of parasites which
326suggests that alkaline induced *Toxoplasma* may be more heterogeneous than
327previously thought. Thus, scRNA-seq resolves a transcriptomic landscape of asexual
328development and suggests the existence of an otherwise hidden state.
329 To determine the reproducibility of the phenomena we observed in the
330differentiating Pru strain parasites, we repeated the analysis with another widely used
331Type II strain, ME49, examining 1828 single ME49 parasites exposed to alkaline
332conditions to induce switching to bradyzoites. Data from the two experiments were
333computationally aligned using Scanorama to remove technical batch effects while
334retaining sample-specific differences[52]. Unsupervised clustering revealed 5 distinct
335clusters in ME49 which share significant overlap in expression patterns with Pru (**Figure**
336**3 - Supplementary Figure 7a**). Matrix correlation of batch-corrected expression across
337the two strains demonstrate analogous mapping for most, but not all cluster identities
338(**Figure 3 - Supplementary Figure 7b**). To simplify the visualization and comparison
339across the two datasets, we next applied Partition-Based Graph Abstraction (PAGA) to
340present clusters of cells as nodes with connectivity based on similarity of the
341transcriptional profiles between clusters[53]. A side-by-side comparison of expression of

342tachyzoite, bradyzoite, and sexual stage specific genes reveals some key similarities
343and dissimilarities (**Figure 3 - Supplementary Figure 7c**). Clusters P1 and M1 are both
344enriched for the expression of bradyzoite marker genes, while clusters M4-5 and P4-5
345are both predicted to be S/M/C phases of the cell cycle. Curiously, P6-specific genes
346(green panels in **Figure 3 - Supplementary Figure 7c**) are not enriched in any cluster
347in ME49, suggesting that P6 state is not conserved across the two type II strains. Such
348differences may not be surprising, however, as Pru and ME49 have entirely distinct
349passage histories.

350**scRNA-seq characterizes surface antigenic repertoire of *Toxoplasma***

351 A unique advantage of scRNA-seq over bulk RNA-seq is its ability to measure
352cell-to-cell variation that is independent of known biological processes. The *Toxoplasma*
353*gondii* genome encodes a family of over 120 SAG1-related sequence (SRS) proteins
354that fall into distinct subfamilies; most or all of these are presumed to be surface
355antigens based on their sequence similarities, including the presence of a predicted
356GPI-addition signal[54]. Whether *SRSs* constitute an antigenic repertoire that contribute to
357evasion of host adaptive immunity response is unclear; however, existing data on
358developmentally regulated expression of *SRSs* including *SAG1* (*SRS29B*) and *SRS16B*
359lend support to that hypothesis[55,56]. In the experiments using 384-well plates, we noted
360that most *SRS* genes were detected in only a few sporadic cells (**Figure 4 –**
361**Supplementary Figure 8a**); however, biological variation was difficult to distinguish
362from measurement dropout (failure to capture a mRNA molecule) given the limited
363sensitivity of 384-well assay and the relatively low abundance of *SRS* transcripts. To
364increase our sensitivity, therefore, we performed scRNA-seq of extracellular
365*Toxoplasma* in 96-well plates which achieved ~40% sensitivity of detection for single
366molecules of ERCC spike-ins, compared to 14% sensitivity that we obtained in the 384-
367well experiments, at roughly equivalent sequencing depth (**Figure 4a**). To determine the
368extent of transcriptional variation in *SRS* genes independent of cell cycle or asexual
369development, we isolated RH parasites in G1 state using DNA content stain and FACS
370(**Figure 4 – Supplementary Figure 8b**). We noticed that the distributions of DNA
371content in single cells varied across the two experiments (compare Figure 4 -
372Supplementary Figure 8b to Figure 2 - Supplementary Figure 3 a), suggesting that the
373distribution may depend on external factors such as tissue culture confluence, parasite
374load, or the amount of time passed since infection. We also measured on average 984
375genes with read counts equal to or greater than two in 96-well plates, up from 862
376genes in 384-well plates (**Figure 4 – Supplementary Figure 8c**). Analysis of the
377resulting 96-well plates data show that the vast majority of *SRS* genes are detected in
378only a small fraction of the population **(Figure 4b)**, similar to what we observed in 384-
379well experiments. To control for measurement dropout as a cause of such variation, we
380first determine the non-zero median for those genes, i.e., the median expression level in

381cells where any transcript for that gene is detected. We then assess how often we fail to
382detect an ERCC spike-ins that had a similar non-zero median expression level. If the
383failure to detect a *SRS* was due to measurement dropout, then the fraction of cells
384without detection for its transcript should be about the same as for the ERCC spike-in
385with similar non-zero median expression. If, on the other hand, the failure to detect the
386*SRS* transcript is due to underlying biological variation between cells, then we will find a
387lower frequency of cells with detectable transcript for that gene than the ERCC spike-in
388with similar expression. The results show that *SRSs* are indeed detected at a
389substantially lower rate when compared to ERCC spike-ins **(Figure 4c)**, indicating that
390the variation of *SRS* detection cannot be explained by measurement noise. Compared
391to most other genes, *SRSs* are expressed in a significantly smaller fraction of the
392population and at a relatively lower abundance **(Figure 4 – Supplementary Figure 8d-**
393**e)**. To determine whether variation of *SRS* expression is due to cell cycle or asexual
394development, we developed a bootstrapping approach to quantify the dependence of
395expression on a topological network that represents either process **(Materials and**
396**Methods)**. We show that apart from a few known *SRSs*, most *SRSs* do not co-vary with
397cell cycle or asexual development, which suggests that the sporadic nature of *SRS*
398expression may hint at a different biological role for their variation, beyond cell cycle and
399asexual development, as discussed further below **(Figure 4d)**. These results reveal new
400insights into the antigenic repertoire of *Toxoplasma*, which appears far more
401heterogeneous, on a parasite-to-parasite basis, than previously known.

402**Transient expression of AP2IX-1 induces surface antigen switching**

403 In examining our data, we were struck by a lone cell in the 384-well dataset of
404RH that had no detectable level of *SRS29B* (*SAG1*), which was otherwise ubiquitously
405and abundantly expressed in all tachyzoites **(Figure 5a)**. We wondered if this cell was
406damaged or unhealthy but its gene count and read depth were similar to its cohort
407**(Figure 5b)**. Further analysis of this SAG1$^-$ cell's transcriptome revealed that it lacks
408expression of the most abundant tachyzoite-specific and bradyzoite-specific genes;
409instead, its gene expression most closely resembles the sexual stages from cat
410intestinal isolates, including abundant expression of a cat-stage *SRS*, *SRS22C* **(Figure**
411**5c)**. Within the set of genes uniquely expressed in the SAG1$^-$ cell are *AP2IX-1* and
412*AP2III-4* which suggest a possible role for one or both of these transcription factors in
413regulating the transcript differences observed in this outlier. To test this hypothesis, we
414transiently expressed AP2IX-1 under the control of a strong promoter in RH parasites
415**(Figure 5d)**. Consistent with our hypothesis, immunofluorescence assay (IFA) revealed
416a reduction of SAG1 surface protein expression within ~18-20 hours after transfection
417**(Figure 5e-f)**, while quantitative RT-PCR showed significantly higher mRNA expression
418for several of the genes that were upregulated in the SAG1$^-$ cell: namely, 207965,
419222305, 205210, and SRS22C, the latter being over 1000-fold higher in the transfected

420population than control **(Figure 5g)**. Note that the SAG1 transcript levels in the
421transfected population were not substantially lower, as expected because there remains
422a large number of untransfected cells in the population which still express high levels of
423this gene. As *SRS22C* is predicted to be a surface antigen like the rest of *SRS*[41], this
424suggests that AP2IX-1 induction can control the switching of surface antigens. We also
425attempted to express *AP2III-4* that is upregulated in the SAG1^{-} cell but were unable to
426obtain an epitope-tagged version of the gene (which is over 9 kbp, including the
427promoter). Overall, these results demonstrate the ability to infer transcriptional
428regulation from a single parasite cell that has an unusual co-expression pattern,
429revealing AP2IX-1 as a novel transcriptional factor that can alter antigen expression in
430*Toxoplasma*.

431**Comparative analysis of *Plasmodium* and *Toxoplasma* reveals shared expression**
432**programs**

433 *Plasmodium* and *Toxoplasma* are both unusual for their prevalence in humans
434and their complex developmental transition, despite the fact that humans are non-
435definitive hosts for both pathogens. *Toxoplasma* has been used as an experimental
436model for other apicomplexans including *Plasmodium*, yet the replication modes
437amongst apicomplexans can be very different. For example, asexual replication of
438*Toxoplasma* involves endodyogeny, which is similar to canonical binary fission, in order
439to replicate and divide. Asexual division of *Plasmodium*, on the other hand, involves
440schizogony, a process that entails multiple rounds of DNA replication and nuclear
441division followed by a mass cytokinesis[57,58]. Despite their fundamental differences in cell
442cycle progression, we wondered if our *Toxoplasma* dataset can be combined with the
443Malaria Atlas[33] to provide insights into apicomplexan biology. Toward this end, we first
444identified 1830 one-to-one orthologous genes between *Plasmodium berghei* and
445*Toxoplasma gondii* Pru **(Figure 6 - Supplementary Figure 9a)**. As expected, the vast
446majority of orthologous genes are not surface adhesion factors or effector molecules in
447*Toxoplasma* **(Figure 6 - Supplementary Figure 9b)**. After removing non-orthologous
448genes, we combined the two species' datasets to produce an integrated UMAP
449projection with Scanorama[59]. In this integrated projection space, mutually similar
450clusters of cells in the two datasets are brought close together, while organism-specific
451cell types are not **(Figure 6a)**. Transitional dynamics of the parasitic development are
452preserved in the integrated projection, as separation of the original cluster assignment
453indicates **(Figure 6b)**. We highlight comparative similarity across the two organisms by
454calculating the fraction of cells that share the same topological neighborhood in the
455integrated network of *Plasmodium* and *Toxoplasma* **(Figure 6c)**, revealing striking
456similarity of expression pattern between the two organisms. We discover the concerted
457transcriptional expression of several conserved orthologous gene sets in the life cycles
458of these two parasites **(Figure 6d)**. For example, the pre-erythrocytic stages of

Plasmodium (sporozoite and merozoites) most closely match the “G1 a” stage of *Toxoplasma*. Both parasites at these stages are not actively replicating DNA and express high levels of ribosomal and mitochondrial genes. Meanwhile, the ring stage of *Plasmodium* most closely matches the “G1 b” phase of *Toxoplasma* because they both express high levels of ribosomal genes with minimal expression of IMC-related and microtubule-related genes. Exo-erythrocytic form (EEF), microgametes (male), and trophozoite stages of *Plasmodium berghei* most closely match the “S” phase of *Toxoplasma* cell cycle. This is because they express DNA-replication factors and centrosome components, which are required for condensation and segregation of chromosomes. Intriguingly, the schizont stage of *Plasmodium* most closely resembles the “M” and “C” phases due to the expression of microtubule, centrosome, and IMC genes. A more detailed illustration of these gene sets expression is shown in **Figure 6 – Supplementary Figure 9c**. Our results indicate that while the cellular morphology and replication strategies may differ drastically between the two parasites, the cellular state, as defined by the transcriptomic profiles, can bear striking analogy and resemblance in the course of asexual replication.

An interactive resource for visualizing single-*Toxoplasma* atlas

Toward enabling the larger scientific community to take advantage of the scRNA-seq data we collected on the three *Toxoplasma* strains, we have constructed an interactive single-cell atlas for *Toxoplasma gondii* (http://st-atlas.org) using Bokeh and Javascript. Our atlas resource allows users to visualize the expression pattern of individual cells by providing a gene ID of interest and using the built-in graphical interface toolset. A factor plot displays expression levels within the parasite population based on cell cycle status, cluster identities, days post induction, or other categories. A sub-panel on the bottom left shows additional information for each input gene including translated product, mean, and standard deviation of the expression. Users can selectively highlight a subset of parasites by using a simple click-and-drag interface for further analysis. Example use cases are provided in **Figure 6e-f.** We have also made the raw data available through the atlas website. We hope this will help make our data and results readily accessible for others interested in exploring *Toxoplasma* parasitology.

Discussion

We describe here single-cell RNA sequencing (scRNA-seq) for measurement of mRNA transcripts from individual extracellular *in vitro Toxoplasma gondii*, an obligate intracellular protozoan parasite. The results show that scRNA-seq can reveal intrinsic biological variation within an asynchronous population of parasites. Two types of biological variation could be seen in our asynchronous populations: cell cycle progression and asexual differentiation. We found the existence of two distinct 1N transcriptional states in cycling parasites which we call G_1a and G_1b, concurring with what was previously reported in bulk analyses of *Toxoplasma*[28]. Interestingly, bradyzoites are found predominantly in G_1b but not in G_1a, suggesting the possibility of a putative checkpoint between these two phases that may also play a role in regulating the developmental transition. Our data further shows a small fraction of bradyzoites to be cycling which supports the hypothesis that bradyzoites can in fact divide[22]. Our results showed a very strong correlation between cell cycle and expression of genes encoding proteins in various subcellular organelles, as noted previously using synchronized bulk populations[28]. The results here, however, show an even more dramatic and extreme dependence on cell cycle, allowing refinement of approaches that use such timing to predict a given protein's ultimate organellar destination in the cell[43]. They also extend such analyses to the Type II strains, Pru and ME49, which have not previously been examined in this way.

In addition to the above, we observed some striking and unexpected heterogeneity within asexually developing parasites. We discovered a cluster of cells, labeled P6, in the differentiating Pru parasites that is distinct from the rest of the alkaline-induced population of cells. Constituting 21% of the alkaline-induced population, the P6 cluster is marked by a set of genes that were previously detected by bulk transcriptomics in bradyzoites of tissue cysts[51]. Remarkably, while most of these genes have unknown functions, we identified an enriched gene with a predicted AP2 domain, which may contribute to the unique expression pattern observed in this group of parasites. We found that the P6 expression profile is intermediate to P2 tachyzoites and P1 bradyzoite clusters. Interestingly, the genes enriched in P6 overlap with a subset of canonical bradyzoite marker genes including *LDH2* and *SRS35A*, albeit expressed at a lower level than in P1 (**Figure 3c**). In addition, we observed a gradual increase in the proportion of P6 cells as induction proceeded from day 3 to day 7. Taken together, one possible explanation for the emergence of P6 cluster is a reverted conversion from bradyzoites to tachyzoites in which alkaline stress fails to maintain the bradyzoite state. Our data and previous reports are consistent with this interpretation[60]. On the other hand, we cannot rule out the possibility that this cluster is developmentally "confused" by the presence of a general stressor such as alkaline. RNA velocity analysis in the Pru data does not reveal a strong transcriptional flow between P1 and P6. Rather, P6

529appears to transcriptionally transition from P2 tachyzoites. Thus, the P1 bradyzoites and
530P6 parasites are either distinct and separate developmental trajectories, or the transition
531from P1 to P6 is a rapid and rare event. Regardless, our results reflect a surprising
532diversity in an asexually transitioning population of *Toxoplasma*. Future measurement of
533single parasites isolated from *in vivo* sources coupled with genetic manipulation of the
534parasite genome, will further clarify the underlying developmental states that we
535identified here.
536 To quantify the variation of *SRSs*, which are generally expressed at low copy
537number, we performed 96-well Smart-seq2, which greatly improved measurement
538sensitivity over the 384-well format, likely due to changes in the input mRNA
539concentration. For scRNA-seq of pathogens, which tend to have smaller size and lower
540mRNA content than mammalian cells, we think a careful selection of the measurement
541approach is necessary based on consideration of throughput and measurement
542sensitivity, between which there is often a tradeoff. Combined with a novel approach
543that we developed based on random permutation and K-nearest neighbor (KNN)
544averaging, we were able to quantify the association of gene expression variation to
545known biological processes, like cell cycle and development. We discovered that
546*Toxoplasma* exhibits unexplained, sporadic variation in the expression of most *SRSs*,
547which may have biological implications. For example, it could expand the mode of
548interactions with the host and be the result of strong selective pressure to maximize
549invasion efficiency and transmission in a variety of different host species of cell types.
550Maintaining a large phenotypic diversity can be beneficial in ensuring at least some
551members will be able to invade the cells it encounters and/or evade adaptive immune
552response, enabling propagation in whatever the host environment encountered.
553 Very surprisingly, our scRNA-seq analysis identified an atypical co-expression
554pattern in an *in vitro* RH “tachyzoite” that is indicative of sexual development, which has
555not been previously observed in these culture conditions. This suggests that at least the
556beginnings of sexual developmental can spontaneously occur even in the absence of
557the cat intestinal environment or other chemical cues. Combined with transient
558expression experiments, the data from this cell enabled us to show that AP2IX-1 is
559sufficient to drive a switching of surface antigen expression toward that resembling the
560sexual stages of the parasite. Assuming this change in mRNA abundance translates into
561a change in protein levels of TGGT1_222305, which is predicted to contain a
562transmembrane domain, and SRS22C, which is strongly indicated to be a surface
563antigen like the rest of SRS, our data indicate that AP2IX-1 contributes to remodeling of
564the surface antigen repertoire during differentiation. Furthermore, this suggests AP2IX-1
565may play a causal role in controlling the sexual differentiation of *Toxoplasma*.
566Considering that the family of AP2 transcription factors was originally found to regulate
567stress response and floral sexual differentiation in plants, our finding suggests the
568biological role of AP2 family in *Toxoplasma* is evolutionarily conserved. Switching of
569surface antigens in parasites may be particularly favorable to parasites under stressful

570conditions, perhaps including the stress of an immune response, thereby enabling
571evasion of host immunity. Regardless, these results show that scRNA-seq can reveal
572rare parasite variants that are, presumably, a result of spontaneous epigenetic changes
573similar to what has been described in cancer cells[61] or transcriptional noise which was
574previously characterized in *Escherichia coli*[62]. An important difference from the situation
575with cancer cells, however, is that these individual variants may be non-viable and so
576impossible to obtain as a stable line; thus scRNA-seq may be uniquely able to provide a
577detailed understanding of their very interesting and informative gene expression. In this
578case, a previously uncharacterized AP2 factor was revealed and shown to be
579responsible for regulating at least some of the genes that were uniquely expressed in
580this variant, relative to the remainder of the tachyzoites in this population. Expanding the
581number of AP2 transcription factors (totaling over 68 of them) analyzed in this way could
582enable the deduction of the sets of “regulons” in this parasite. Thus, even though these
583rare variants may be non-viable “biological freaks”, they can be highly informative and
584would be completely undetectable in bulk measurement.
585 Recently, cross-species analysis of scRNA-seq datasets has attracted
586considerable interest[63,64]. Our study provides the first comparative analysis of
587developmental processes between two apicomplexans, both of which cause prevalent
588and potentially devastating diseases. While *Plasmodium* and *Toxoplasma* undergo
589distinct modes of cell replication and asexual development, we identified cross-species
590clusters that share significant similarity in the expression of orthologous genes. We
591discovered that the timing of expression in gene sets involved in cell cycle are
592conserved in the erythrocytic cycle of *Plasmodium berghei*. Lastly, we have made the
593datasets of our study available by creating an interactive and easily accessible web-
594browser. We hope this encourages other individuals interested in single-cell
595parasitology to actively explore our dataset without having expertise in programming or
596bioinformatics. Building on the work described here, which lays a foundation for a
597detailed understanding of the parasite itself, we anticipate future, single-cell co-
598transcriptomic sequencing of both the host cell and the parasite as a potentially
599powerful approach to further deconstruct the complexity of parasite-host interactions.

Materials and Methods

Key Resources Table

Reagent type (species) or resource	Designation	Source or reference	Identifiers	Additional information
Cell line (Toxoplasma gondii)	ME49	PMID: 15664907		
Cell line (Toxoplasma gondii)	Pru	PMID: 18347037		
Cell line (Toxoplasma gondii)	RH mCherry / RH	This work.		
Cell line (Toxoplasma gondii)	RH Δhxgprt	PMID: 8662859		
Cell line (Toxoplasma gondii)	RH GFP	Gift of Michael W Panas.		
Recombinant DNA reagent	pGRA-AP2IX1-V5	This work.		Constitutive expression plasmid carrying AP2IX1 in tandem fusion to V5 tag.
Chemical compound, drug	Propidium iodide (PI)	ThermoFisher	P3566	
Chemical compound, drug	Sytox Green	ThermoFisher	S7020	
Chemical compound, drug	Fixable blue dead cell stain kit	ThermoFisher	L34962	
Chemical compound, drug	Vybrant DyeCycle Violet (DCV)	ThermoFisher	V35003	

Chemical compound, drug	VECTASHIELD Antifade Mounting Medium with DAPI	Vector Laboratories	H-1200-10	
Chemical compound, drug	Nuclease-free water	IDT	11-04-02-01	For SmartSeq2 protocol
Chemical compound, drug	recombinant RNase inhibitor	Takara Clonetech	2313A	For SmartSeq2 protocol
Chemical compound, drug	10 mM dNTP	ThermoFisher	R0194	For SmartSeq2 protocol
Chemical compound, drug	ERCC RNA Spike-in Mix	ThermoFisher	4456740	For SmartSeq2 protocol
Chemical compound, drug	10% Triton X-100	Sigma-Aldrich	93443	For SmartSeq2 protocol
Chemical compound, drug	Buffer EB (elution buffer)	QIAGEN	19086	For SmartSeq2 protocol
Chemical compound, drug	AMPure XP nucleic acid purification beads	Beckman Coulter	A63880	For SmartSeq2 protocol
Chemical compound, drug	Nucleofector Solution	Lonza	P3 Primary Cell solution	For transient transfection of *Toxoplasma gondii*
Antibody	Rabbit anti-SAG1 polyclonal antibody	PMID: 15944311		(1:500)
Antibody	Mouse anti-V5 tag monoclonal antibody	Invitrogen	R960-25	(1:1000)
Antibody	Goat polyclonal Alexa 488 Fluor-conjugated secondary antibodies	Invitrogen	A28175	(1:1000)
Commercial assay, kit	SsoAdvanced	Bio-rad	1725271	qPCR mastermix

	Universal SYBR Green Supermix			
Sequence-based reagent	All oligos used in this study	See "supplementary_file1_oligos.csv"		
Software	Analysis algorithm	www.github.com/xuesoso/singleToxoplasmaSeq		
Software	Interactive browser	st-atlas.org		

Cell and Parasite Culture

All *Toxoplasma gondii* strains were maintained by serial passage in human foreskin fibroblasts (HFFs) cultured at 37 C in 5% CO_2 in complete Dulbeco's Modified Eagle Medium (cDMEM) supplemented with 10% heat-inactivated fetal bovine serum (FBS), 2 mM L-glutamine, 100 U/ml penicillin, and 100 ug/ml streptomycin. *T. gondii* strains used in this study were RH, Pru-GFP, and ME49-GFP-luc.

In vitro Bradyzoite Switch Protocol

Differentiation to bradyzoite was induced by growth under low-serum, alkaline conditions in ambient (low) CO_2 as previously described[65]. Briefly, confluent monolayers of HFFs were infected with tachyzoites at a multiplicity of infection (MOI) of 0.025 in RPMI 1640 medium (Invitrogen) lacking sodium bicarbonate and with 1% FBS, 10 mg/ml HEPES, 100 U/ml penicillin, and 100 g/ml streptomycin at pH 8.2. The infected HFFs were cultured at 37°C without supplemented CO_2.

Preparation of Parasites for Fluorescence Activated Cell Sorting (FACS)

HFF monolayers infected with parasites overnight were scraped, and the detached host cells were lysed by passing them through a 25-gauge needle three times or a 27-gauge needle six times. The released parasites were spun down at 800 rpm for 5 minutes to pellet out host cell debris, and the supernatant was spun down at 1500 rpm for 5 minutes to pellet the parasites. The parasites were then resuspended in 500 µL of FACS buffer (1x phosphate-buffered saline, PBS, supplemented with 2% FBS, 50 ug/ml DNAse I, and 5 mM $MgCl_2$*$6H_2O$), passed through both a 5 µm filter and a filter cap into FACS tubes, and stored on wet ice until it was time to sort. In samples stained for DNA content, the parasites were resuspended in 500 µL of FACS buffer plus 1.5 µL of

629Vybrant DyeCycle Violet (from ThermoFisher, catalog number V35003) and incubated at
63037 C and 5% CO_2 for 30 minutes.
631 The parasites were also stained with either propidium iodide (PI), Sytox Green,
632or the live/dead fixable blue dead cell stain kit (catalog number L34962) prior to sorting
633in order to distinguish live cells from dead cells. To stain with PI, 10 µL of 0.5 mg/ml PI
634was added to every 500 µL of parasite suspension in FACS buffer, and the parasites
635were incubated covered on ice for at least 15 minutes. To stain with Sytox Green, 1 drop
636of Sytox Green per ml was added to the parasite suspension in FACS buffer, and the
637parasites were incubated at room temperature for at least 15 minutes. To stain with the
638live/dead fixable blue dead cell stain kit, 1.5 µL of the kit's viability dye was added to
639every 500 µL of parasites along with the secondary antibody, and parasites were
640washed and resuspended in FACS buffer as usual.
641
642*FACS of parasites*
643 Eight mL of lysis buffer was prepared by mixing together: 5.888 mL of water, 160
644µL recombinant RNase inhibitor (Takara Clonetech), 1.6 mL of 10 mM dNTP
645(ThermoFisher), 160 µL of 100 uM oligo-dT (iDT; see attached
646"supplementary_file1_oligos.csv" for oligos), 1:600,000 diluted ERCC spike-in
647(ThermoFisher), and 32 µL of 10% Triton X-100. All reagents are declared RNase free.
648Lysis plates were prepared by dispensing 0.4 µL of lysis buffer into each well of a 384
649well hard-shell low profile PCR plate (Bio-rad) using liquid handler Mantis (Formulatrix).
650Single parasites were sorted using the Stanford FACS Facility's SONY SH800s sorter or
651BD Influx Special Order sorter into the 384-well plates loaded with lysis buffer. Single
652color and colorless controls were used for compensation and adjustment of channel
653voltages. The data were collected with FACSDiva software and analyzed with FlowJo
654software. RH parasites were index sorted with fluorescence signal of cell permeable
655DNA stain, DyeCycle Violet.
656
657*Single-Toxoplasma cDNA synthesis, library preparation, and sequencing*
658 Smart-seq2 protocol was carried out as previously described[66] using liquid
659handlers Mantis and Mosquito (TTP Labtech) with slight modifications. 384-well Smart-
660seq2 was performed with a 2 µL final reaction volume, while 96-well format was carried
661out in 25 µL final reaction volume as recommended by the original protocol. For 384-
662well Smart-seq2, we performed 19 rounds of cDNA pre-amplification after reverse
663transcription with oligo-dT primers. Each well is then diluted with 1 to 4 v:v in RNAse
664free elution buffer (QIAgen) to a total volume of 8 µL. For 96-well Smart-seq2, we
665performed 30 rounds of cDNA pre-amplification after reverse transcription. PCR is
666performed with "IS_PCR primers". Each well is then purified with Ampure XP beads at
6670.8X volume ratio and resuspended in 20 µL RNAse free elution buffer. We measured
668the size distribution and concentration of each well in 96-well plate using Fragment
669Analyzer High-sensitivity NGS kit (Agilent). We normalized the concentration of cDNA of

670each well to a concentration of 0.4 ng/µL. Finally, for both 384-well and 96-well Smart-
671seq2 measurements, we conducted library preparation with in-house Tn5 tagmentation
672using custom cell barcode and submitted for 2 x 150 bp paired-end sequencing on
673NovaSeq 6000 at the Chan Zuckerberg Biohub Genomics core. All primer sequences
674are provided as a supplementary file.
675
676*AP2IX-1 transient expression*
677 The pGRA-AP2IX1-V5 plasmid for AP2IX1 transient expression was created
678using Gibson assembly (NEB) from the pGRA-V5[67]. RH parasites were transfected with
679pGRA-AP2IX1-V5 using the Amaxa 4D Nucleofector (Lonza). Tachyzoites were
680mechanically released in PBS, pelleted, and resuspended in 20 µL P3 Primary Cell
681Nucleofector Solution (Lonza) with 7 or 15 µg DNA for transfection. After transfection,
682parasites were allowed to infect HFFs in DMEM. After 18-20 hours of infection,
683parasites were prepared for Immunofluorescence Assay (IFA) or qRT-PCR. To compute
684statistical independence between the transfected and control samples, we applied
685Student's t-test by assuming unequal variance. One sigma (*) indicates one standard
686deviation in mean difference assuming null hypothesis.
687
688*Immunofluorescence Assay (IFA) quantification*
689 Monolayers of infected cell on glass coverslips were fixed with cold methanol for
69012 minutes. Samples were washed with PBS and blocked using 3% bovine serum
691albumin (BSA) in PBS for at least 30 minutes. SAG1 was detected with rabbit anti-
692SAG1 polyclonal antibody and V5 was detected with mouse anti-V5 tag monoclonal
693antibody (Invitrogen). Primary antibodies were detected with goat polyclonal Alexa
694Fluor-conjugated secondary antibodies (Invitrogen). Primary and secondary antibodies
695were both diluted in 3% BSA in PBS. Coverslips were incubated with primary antibodies
696for 30 minutes, washed, and incubated with secondary antibodies for 30 minutes.
697Vectashield with DAPI stain (Vector Laboratories) was used to mount the coverslips on
698slides. Fluorescence was detected using wide-field epifluorescence microscopy and
699images were analyzed using ImageJ. All images shown for any given condition/staining
700in any given comparison/dataset were obtained using identical parameters.
701
702*Quantitative polymerase chain reaction (qPCR)*
703 To quantify the purity of single parasite sort and to ensure the cDNA synthesis
704reaction was not saturated, GFP, mCherry, or SAG1 mRNA expression were measured
705using commercial qPCR mastermix, SsoAdvanced™ Universal SYBR Green mastermix
706(Bio-rad). Briefly, 0.1 µL of diluted cDNA was added in a total of 2.1 µL reaction volume
707per well on a 384 well plate with qPCR mastermix and 200 nM PCR primers. The
708reaction was incubated on a Bio-rad qPCR thermal cycler with the following programs: 5
709minutes of 95ºC, 45 cycles of 95ºC for 5 seconds and 56ºC for 1 minute, and imaging.
710To quantify the transcriptional effects of AP2IX-1 transient expression in RH parasites,

711infected cell monolayers were first lysed with Trizol (Invitrogen) and RNA was extracted
712using standard molecular biology technique. cDNA from each sample was generated
713with Smart-seq2 protocol using 20 µL total reaction volume and roughly 200 ng RNA
714input followed by 0.8X AMPure XP beads (Beckman Coulter) purification. For qPCR, 1
715ng of cDNA was added in a total of 2.1 µL reaction volume per well on a 384 well plate
716with qPCR mastermix and 200 nM PCR primers as described above. The reaction was
717incubated on a Bio-rad qPCR thermal cycler with the following programs: 5 minutes of
718$95^{o}$C, 60 cycles of 95°C for 5 seconds and 61°C for 30 seconds, and imaging. Each
719gene was measured four times with samples collected from at least two separate wells.
720The transfection and qRT-PCR experiments were performed twice in separate
721experiments. Fold change of gene expression was calculated as shown previously[68]
722using ACT1 expression as an internal control for samples. All primer sequences are
723provided in “supplementary_file1_oligos.csv”.
724
725*Sequencing alignment*
726 BCL output files from sequencing were converted into gzip compressed FastQs
727via a modified bcl2fastq demultiplexer which is designed to handle the higher
728throughput per sequencing run. To generate genome references with spike-in
729sequences, we concatenated T. gondii ME49 NCBI genome assembly version
730011/1/2013 or T. gondii GT1 T NCBI Genome assembly version 7/19/2013 genome
731references with ERCC sequences (obtained from ThermoFisher website). The raw fastq
732files from sequencing are aligned to the concatenated genomes with STAR aligner
733(version 2.6.0c) using the following settings: “--readFilesCommand zcat --outFilterType
734BySJout --outFilterMutlimapNmax 20 --alignSJoverhangMin 8 --alignSJDBoverhangMin
7351 --outFilterMismatchNmax 999 --outFilterMismatchNoverLmax 0.04 --alignIntronMin 20
736--alignIntronMax 1000000 --alignMatesGapMax 1000000 --outSAMstrandField
737intronMotif --outSAMtype BAM Unsorted --outSAMattributes NH HI AS NM MD --
738outFilterMatchNminOverLread 0.4 --outFilterScoreMinOverLread 0.4 --
739clip3pAdapterSeq CTGTCTCTTATACACATCT --outReadsUnmapped Fastx”.
740Transcripts were counted with a custom htseq-count script (version 0.10.0,
741https://github.com/simon-anders/htseq) using ME49 or RH GFF3 annotations (version
74236 on ToxoDB) concatenated with ERCC annotation. Instead of discarding reads that
743mapped to multiple locations, we modified htseq-count to add transcript counts divided
744by the number of genomic locations with equal alignment score, thus rescuing
745measurement of duplicated genes in the *Toxoplasma* genome. Parallel jobs of STAR
746alignment and htseq-count were requested automatically by Bag of Stars
747(https://github.com/iosonofabio/bag_of_stars) and computed on Stanford high-
748performance computing cluster Sherlock 2.0. Estimation of reads containing exonic and
749intronic regions is computed with Velocyto estimation on the BAM output files and
750requested automatically by Bag of Velocyto
751(https://github.com/xuesoso/bag_of_velocyto) on Sherlock 2.0. Gene count matrix is

obtained by summing up transcripts into genes using a custom python script. Scanpy velocyto package is then used to estimate transcriptional velocity on a given reduced dimension. Parameters used for generating the results are supplied as supplementary python scripts. Sample code to generate the analysis figures are provided in supplementary jupyter notebooks.

Data preprocessing

To filter out cells with poor amplification or sequencing reaction and doublet cells, we discarded cells based on gene counts (>0 reads), total reads sum, percent reads mapped to *Toxoplasma* genome, percent ERCC reads, and percent ribosomal RNA reads. We reported "% mapped" based on the meta-alignment output from STAR aligner. We checked for some of the unmapped reads on BLASTn and found the majority of them to map to Toxoplasma 28S ribosomal RNA. Next, we filtered “ribosomal RNA” genes from the gene count matrix. Gene count matrices are normalized as counts per median (CPM):

$$X_{norm} = \frac{X}{\sum(X)} \cdot median(\sum(X)) \qquad (1)$$

where *X* is the gene count matrix, *sum(X)* is the read sum for each cell, and *median(sum(X))* is the median of read sums. Normalized data are added with a pseudocount of 1 and log transformed (e.g. $\log_2(X_{norm}+1)$). To determine the detection limit (e.g. 50% detection rate), we modeled the detection probability of ERCC standards with a logistic regression as a function of spike-in amount[34].

We calculated an estimate of absolute molecular abundance for all genes by fitting a linear regression to ERCC spike-ins:

$$log_2(Y) = m \cdot log_2(X_{norm} + 1) + b \qquad (2)$$

where $X_{norm,\ ERCC>0.5}$ is the observed CPM value for ERCC spike-ins above the detection limit, *Y* is the amount of ERCC spike-in, *m* is the regression coefficient, and *b* is the intercept. To reduce the influence of measurement noise, we fit the model only to ERCC spike-ins with mean expression above the detection limit.

Cell cycle analysis and annotation

To determine the transcriptional variation associated with cell cycle, we applied Self-Assembling Manifolds (SAM)[69] to filter for highly dispersed gene sets (>0.35 SAM weights) in asynchronous RH population. Principal components analysis (PCA) is then applied to the filtered and normalized RH data, and the nearest neighbor graph (K=50) is computed using “correlation” as a similarity metric. We identified the putative “G1”

clusters with 1N based on DNA content stain. Parasites in “G1” cluster are further sub-clustered with Louvain Clustering, in which we identified “G_1a” and “G_1b” clusters with distinct transcriptional profiles. Pearson correlation between single-cell and bulk transcriptomic data is computed between bulk assignment[28] and the scRNA-seq cluster assignment through which each cluster is uniquely assigned with a cell cycle state. To quantify genes that are differentially expressed across cell cycle clusters, we applied Kruskal-Wallis test. Genes are considered differentially expressed if their p-values are less than 0.05 and they are at least 2-fold over-expressed in a cluster compared to the average expression level of other clusters. We computed differential expression across all cell cycle clusters as well as between the “G_1a” and “G_1b” clusters; the results are uploaded as supplementary files 2 and 3, respectively. To enable cell cycle assignment transfer from RH to Pru and ME49 data, we implemented a random forest classification model trained on RH data. Briefly, this is done by training a model with 1000 estimators on L2-normalized RH expression data containing only cell cycle associated genes in a 60-40 split scheme. Then the model is applied to predict cell cycle labels of L2-normalized Pru or ME49 data containing the homologous cell cycle associated genes. The testing accuracy was over 95%.

Pseudotime construction and clustering

Pseudotime analysis is conducted with Monocle 2 package in R on preprocessed dataset with highly dispersive genes as described previously. A cell in “G_1a” is designated as the root cell, and all other cells are placed after this cell in order of their inferred pseudotime. To cluster genes based on their pseudotime expression pattern, high frequency patterns are removed through a double spline smoothing operation. The interpolated expression matrix is then normalized by maximum expression along pseudotime such that the maximum value of gene expression along pseudotime is bound by 1. We then applied agglomerative clustering on this interpolated and normalized expression matrix using “correlation affinity” as similarity metric and “average linkage” method to predict three distinct clusters of genes.

Projection dependence scoring

To quantify the dependence of expression variation on a two-dimensional projection, we developed a novel approach based on k-nearest neighbor (KNN) averaging. First, a KNN graph is computed by locating nearest neighborhood in a projection using euclidean distance. We then generated a null expression matrix by shuffling the gene expression matrix along each cell column, such that its correlation with respect to the coordinate on projection is completely lost. Next, we compute an updated gene expression value by taking the average of expression values across the KNN. This is equivalent to:

$$X_{KNN} = \frac{M}{k} \cdot X_{norm} \quad (3)$$

where X_{KNN} is the updated KNN averaged expression, M is the nearest-neighbor graph with k being the number of nearest neighbor, and X is the log-transformed CPM of observed or null expression matrices. We chose a k of 5 for all our analysis as varying k did not have a large effect on the results (data not shown). In our experiments, we have shown that the first two principal components (PCs) of PCA on RH correspond to the projection of cell cycle progression, and a two-dimensional UMAP projection of Pru corresponds to asexual development and cell cycle progression. We thus computed X_{KNN} for both the original, observed expression matrix and the shuffled, null matrix on either projection to reflect dependence on cell cycle progression and/or asexual development. X_{KNN} is further normalized to have identical sum as the original expression values. A Kolmogorov-Smirnoff two sample test is then computed between the normalized X_{KNN} of the observed matrix and that of the shuffled matrix based on 100 random permutations. The projection-dependence score for each gene is then computed as:

$$S_g = \sqrt{-\log(\bar{P}_g)} \quad (4)$$

where S_g is the projection-dependence score for gene g and $\bar{P}_g$ is the average p-values of 100 tests. We present S_g normalized by the maximum score within each respective data set.

Comparative Analysis of Plasmodium and Toxoplasma scRNA-seq

To integrate scRNA-seq data of *Plasmodium berghei* from Malaria Atlas[33] with our *Toxoplasma* Pru dataset (measured both induced and induced population in 384-well), we first identified one-to-one orthologous genes obtained from PlasmoDB(https://plasmodb.org/) and ToxoDB(https://toxodb.org/toxo/). Next, we filtered each dataset with the ortholog genes. Using scanpy library, we filtered for the intersect of genes that are within the top 800 most dispersed genes in each dataset, resulting in a list of 403 genes. Finally, we used Scanorama[52] with default parameter settings to integrate the two datasets. We calculated co-clustering similarity as follows. We first computed a Leiden[70] clustering on the integrated graph and returned a cluster co-occurrence matrix to the original cluster assignment in *Plasmodium berghei* (“ShortenedLifeStage4”) or *Toxoplasma* Pru (“cell_cylcle”). Then, the dot product between the two matrices was calculated and normalized such that it has a maximum of one.

Data availability

Analysis scripts, preprocessing scripts, and instructions to obtain the processed data are provided on https://github.com/xuesoso/singleToxoplasmaSeq. A sample jupyter notebook that regenerates some of the analysis and figures is provided in the Git repository. Raw fastq and processed files are deposited on GEO and SRA repositories (GSE145080).

Acknowledgements

We thank Fabio Zanini, Felix Horns, and Geoff Stanley for illuminating discussion and advice to YX on experiments and analysis. We thank Saroja Korullu, Robert Jones, and Vickie Lin for assistance with library preparation and sample submission. We thank Meredith Weglarz and Lisa Nichols at the Stanford Beckman FACS facility for assistance with FACS. We thank Michael W Panas for providing Toxoplasma GFP strain used in this study. This study is supported by National Institute of Health (NIH) RO1 AI021423, AI129529, and Chan Zuckerberg Biohub. YX and TCT are supported by Stanford Interdisciplinary Graduate Bio-X Fellowships. SR is supported by NIH F30 AI124589-03. AF is supported by NIH 5T32AI007328-30 and a Gilliam Fellowship for Advanced Study from Howard Hughes Medical Institute.

Figures

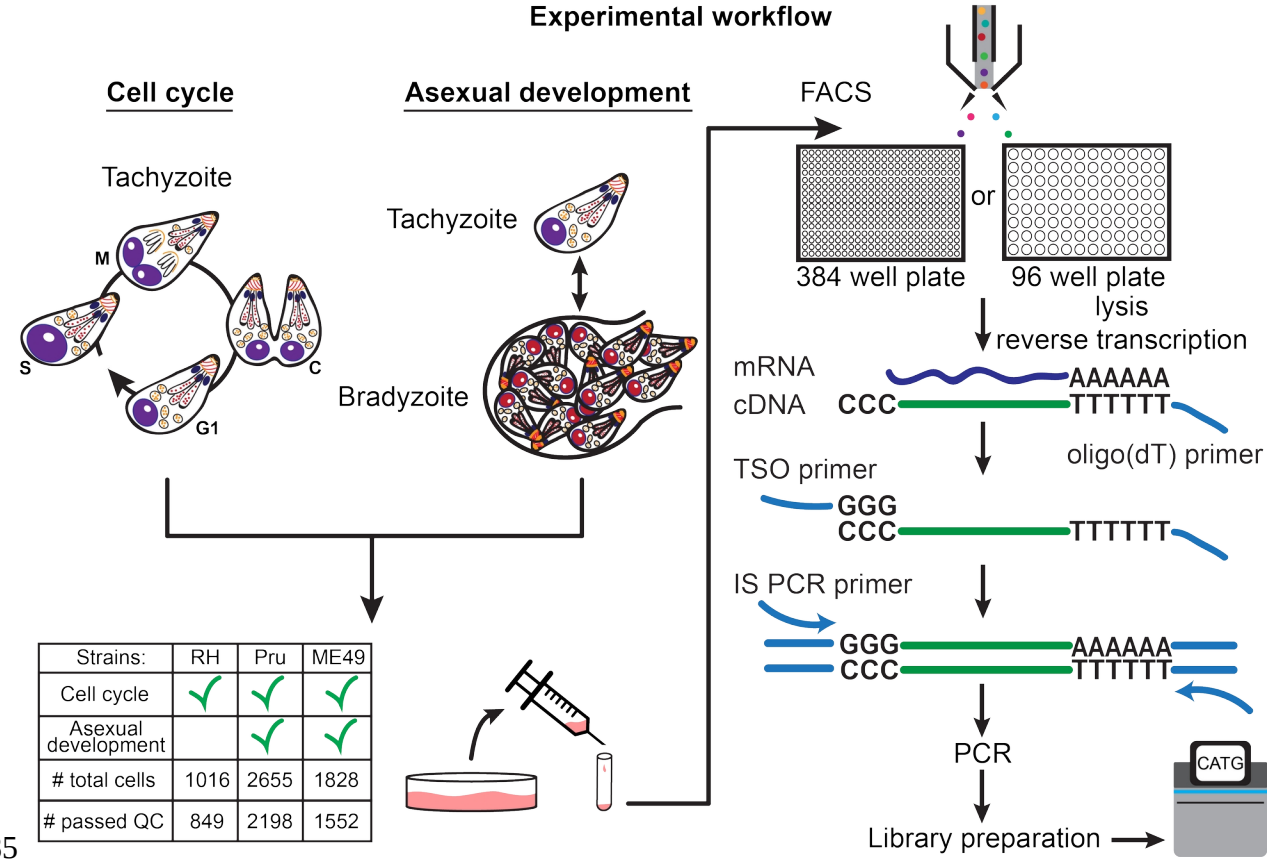

Strains:	RH	Pru	ME49
Cell cycle	✓	✓	✓
Asexual development		✓	✓
# total cells	1016	2655	1828
# passed QC	849	2198	1552

Figure 1. Schematic of single-cell RNA-sequencing (scRNA-seq) based on a modified Smart-seq2 protocol for 384-well or 96-well plate. A table of strain types with the number of sequenced cells and cells that passed quality checking (QC) is provided.

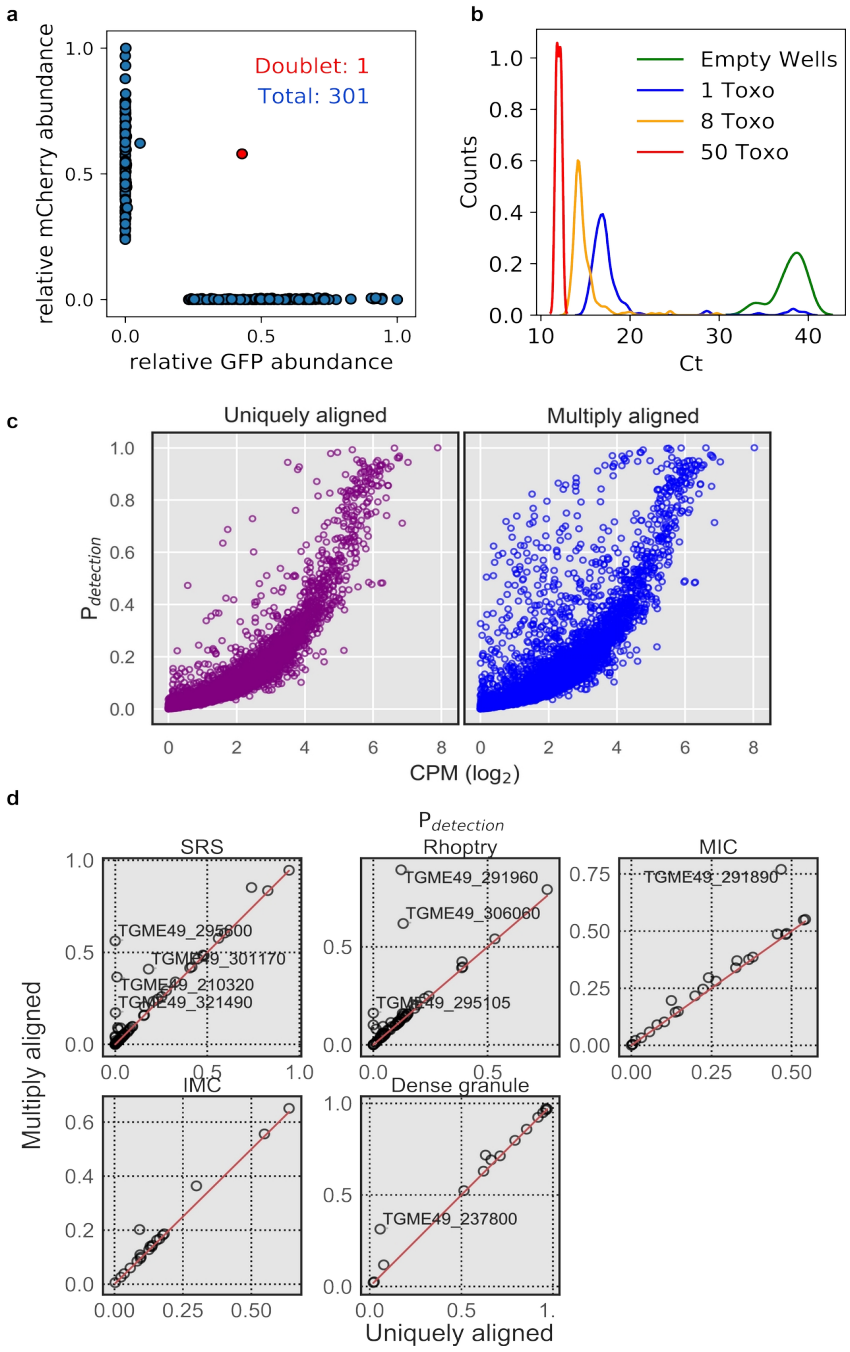

Figure 1 - Supplementary Figure 1. (a) qPCR measurement of mRNA expression in 301 transgenic *Toxoplasma* cells expressing GFP or mCherry mixed at 1:1 ratio. **(b)** qPCR Ct values of abundant surface protein, SAG1, measured for 374 wells with zero, one, eight, or fifty sorted parasites at 16, 176, 176, and 36 replicates, respectively. **(c)** Comparison between "uniquely aligned" (default htseq-count settings) and "multiply aligned" (count each feature with equal read alignment score divided by the number of aligned reads) in the detection rate (≥ 2 read count) in Type I strain, RH. **(d)** A more detailed comparison of detection rate of several parasite-specific gene sets in Pru (uninduced + induced). Genes that are detected more frequently in "multiply aligned" setting are annotated with their gene IDs in the plot.

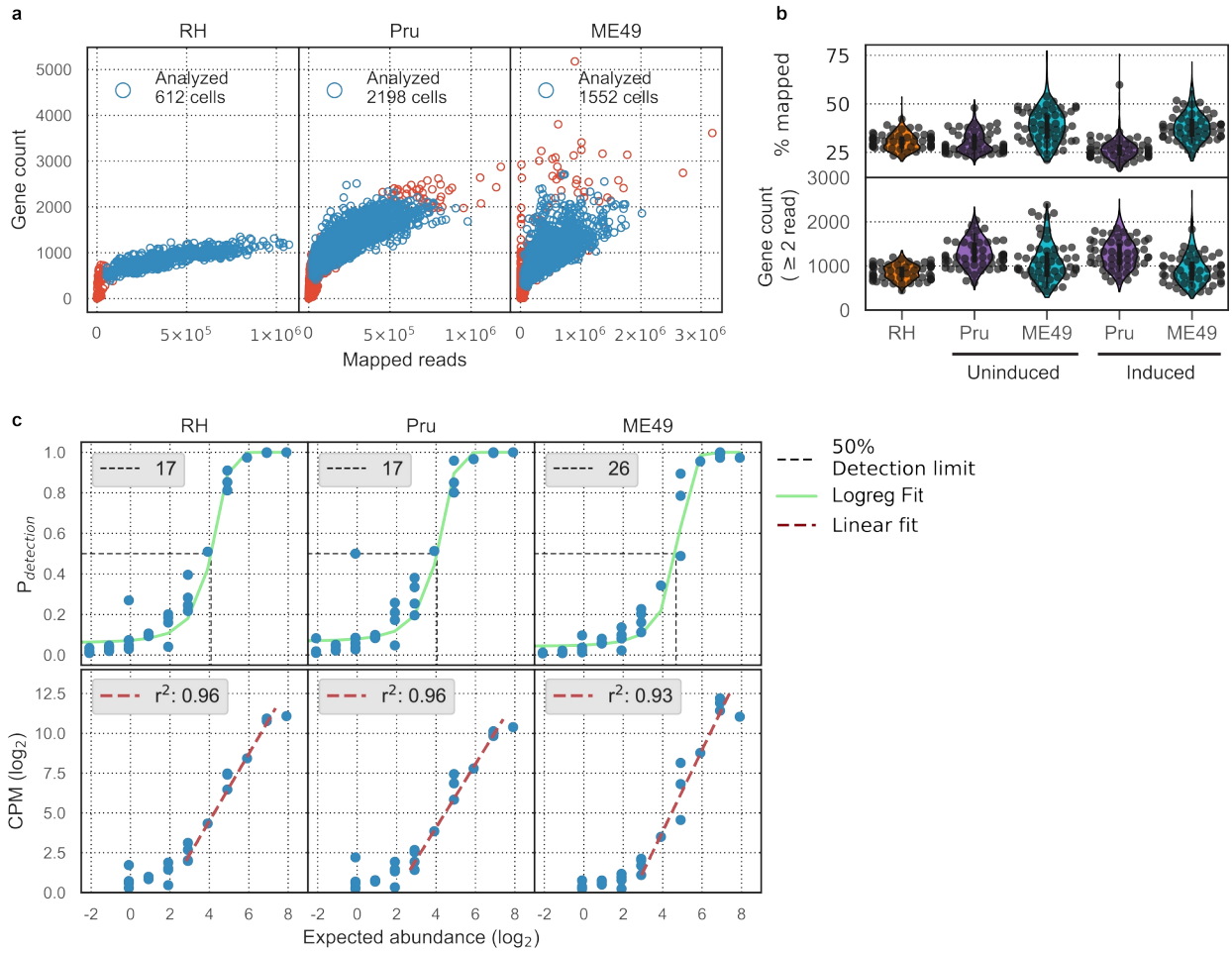

Figure 1 - Supplementary Figure 2. (a) Comparison of gene counts (≥2 read counts) and total mapped read counts for RH, Pru, and ME49 from left to right, respectively. Text in top left corner indicates the number of parasites that passed cell filtering and were analyzed (blue open circles). **(b)** Top panel: distributions of percentage of reads in the analyzed cells that aligned to *Toxoplasma* genome references. Bottom panel: distributions of gene counts (≥2 read counts) in analyzed cells. Uninduced Pru and ME49 were grown in the absence of alkaline (Day 0), whereas induced Pru and ME49 were grown in the presence of alkaline (Day 3 - 7). **(c)** Top panel: Logistic regression modeling (green line) of detection limit (50% detection rate, black dotted line) of ERCC spike-ins. Text on top left of each sub-panel indicates the detection limit in absolute molecular counts. Bottom panel: Linear regression modeling (crimson line) of measurement accuracy fitted on ERCC spike-ins with abundance above the detection limit. Text on top left of each sub-panel indicates the coefficient of determination for the regression fit.

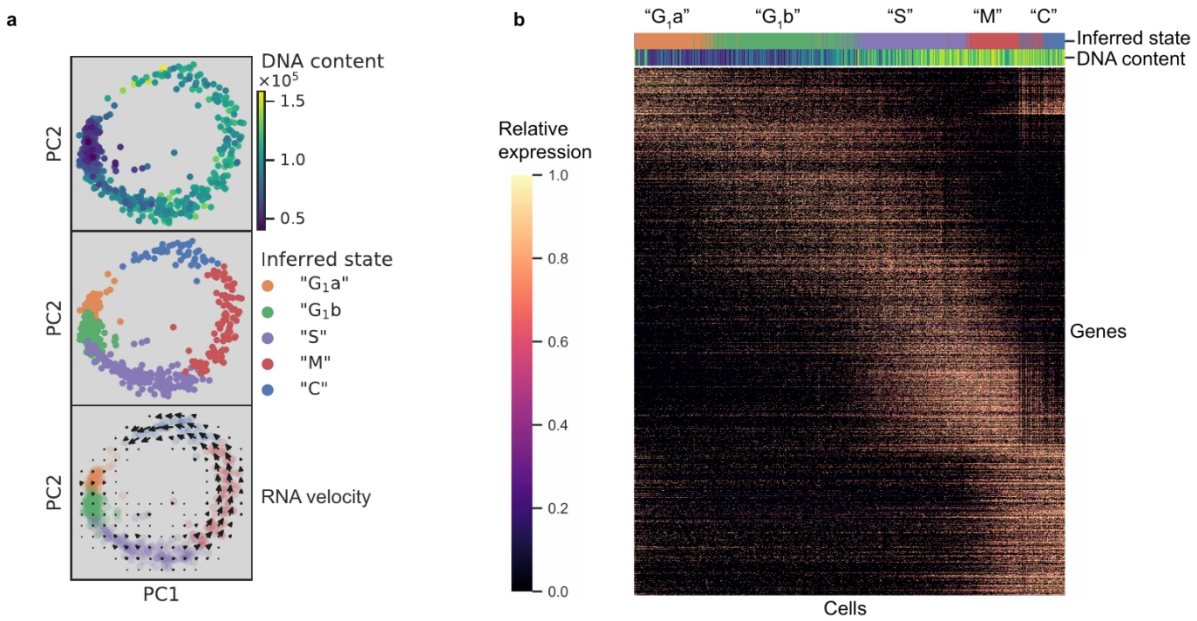

Figure 2. (a) Projection of the first two principal components in RH data set. Top panel: 612 RH cells are colored by fluorescence measurement (arbitrary unit) of a cell permeable DNA content stain, DyeCycle Violet. Center panel: cells are colored by cluster assignment and labeled by the inferred “cell cycle” state. Bottom panel: RNA velocity vector field is overlaid on top of the inferred state colors, with arrows pointing in the direction of net transcriptional change. **(b)** Heatmap of the 1465 most variable gene expression are displayed along the rows. Cells areordered by pseudotime assignment in ascending order along the columns of the heatmap (from left to right). Top colorbar reflects the assignment of inferred state and bottom colorbar reflects the relative fluorescence of DNA content using the same color scheme as in (a).

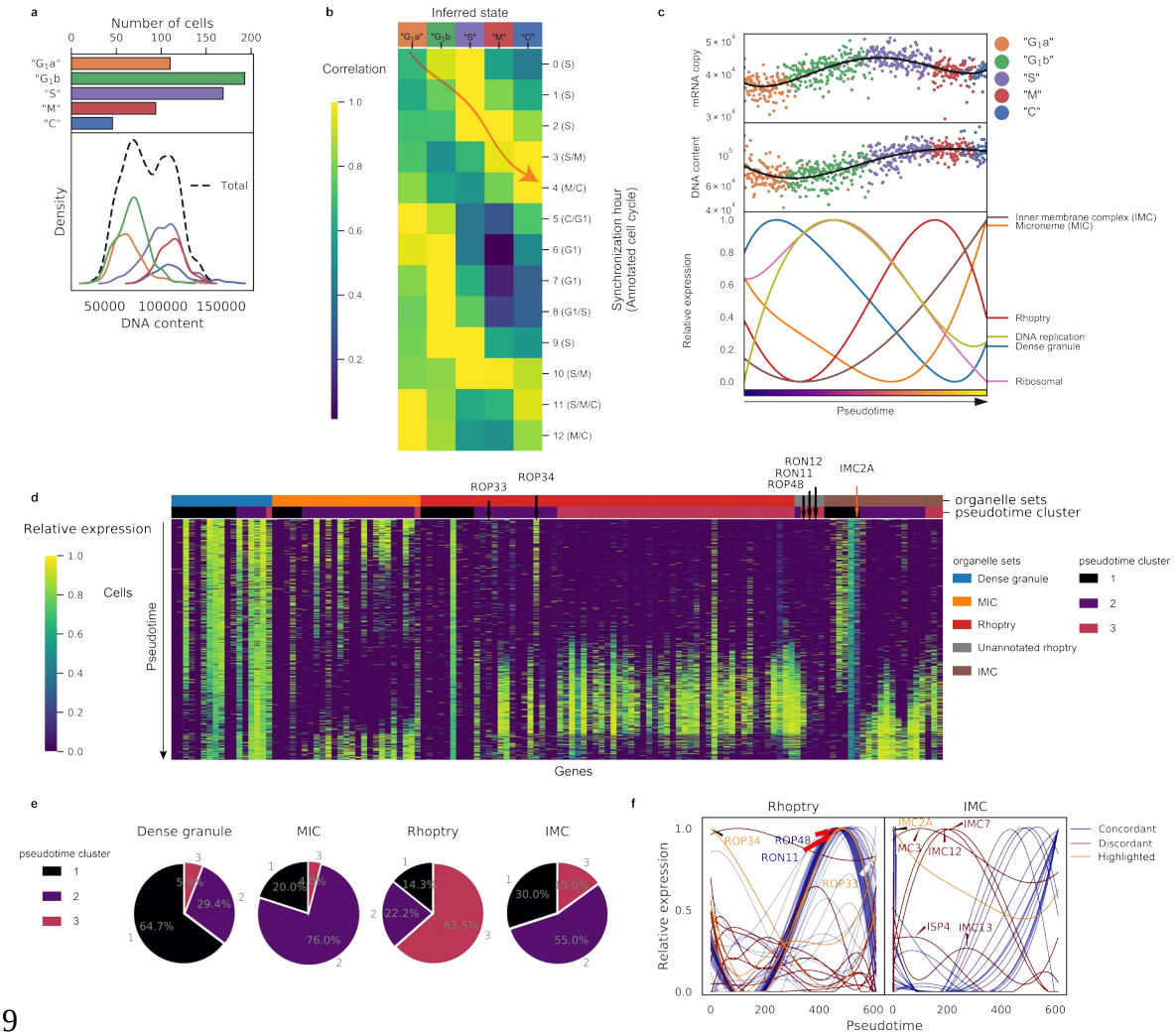

Figure 2 - Supplementary Figure 3. (a) Top panel: Numbers of RH parasites in each inferred "cell cycle" state. Bottom panel: Density plots of DNA content distributions stratified by the inferred state. **(b)** Heatmap of average expression correlation between each inferred "cell cycle" state of RH and each time-point of bulk transcriptomic measurement based on chemically synchronized parasites. **(c)** Absolute mRNA abundance (top panel) and DNA content (center panel) ordered by "cell cycle" pseudotime with individual cells colored by their inferred states. A spline smoothing is applied to approximate a rolling average along the pseudotime (black solid line). Average expression of gene sets based on ToxoDB (v.36) annotation of organellar destination of the protein product after double spline smoothing (bottom panel). **(d)** Heatmap of gene expression ordered by organelle sets (top colorbar) and pseudotime cluster (bottom colorbar). "Unannotated rhoptry" refers to genes not annotated in ToxoDB (v.36) as encoding a rhoptry protein but whose expression pattern is highly concordant with the dominant rhoptry pattern. **(e)** Pie charts of pseudotime cluster frequency for parasite organelle sets. **(f)** Expression of annotated rhoptry (left panel) and inner-membrane complex (IMC; right panel) genes along pseudotime with different colors indicating genes concordant (blue) and discordant (crimson and orange) to the major trend of their organelle sets. Discordant genes which are known to be misannotated are highlighted in orange.

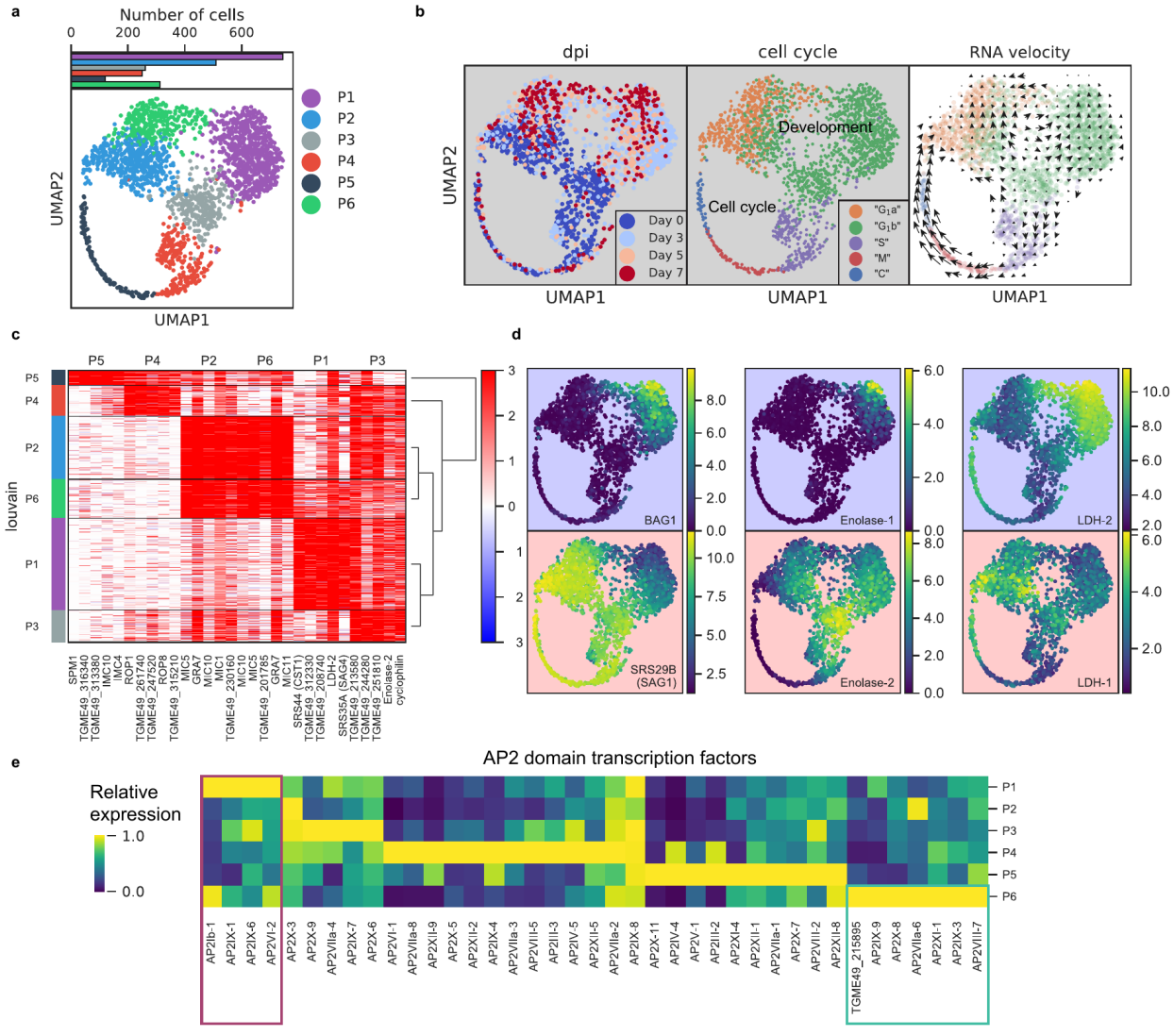

Figure 3. (a) UMAP projection of 809 uninduced and 1389 induced Pru parasites with colors indicating Louvain cluster assignment. Top panel shows the number of parasites in each cluster. **(b)** UMAP projections of Pru parasites colored or labeled by days post induction (dpi), inferred cell cycle states, and RNA velocity from left to right. **(c)** Heatmap of differentially expressed genes (along columns) across Louvain clusters of cells ordered by hierarchical clustering (along rows). The top 5 most enriched genes from each cluster are presented. **(d)** UMAP projections of Pru colored by the neighbor-averaged expression ($\log_2$ CPM) of bradyzoite (top panels, purple background) and tachyzoite (bottom panels, red background) marker genes. **(e)** Heatmap of average expression level of AP2 transcription factors for each Louvain cluster, normalized by the maximum cluster expression level within each AP2. Purple and green rectangles highlight AP2s enriched in clusters P1 and P6, respectively.

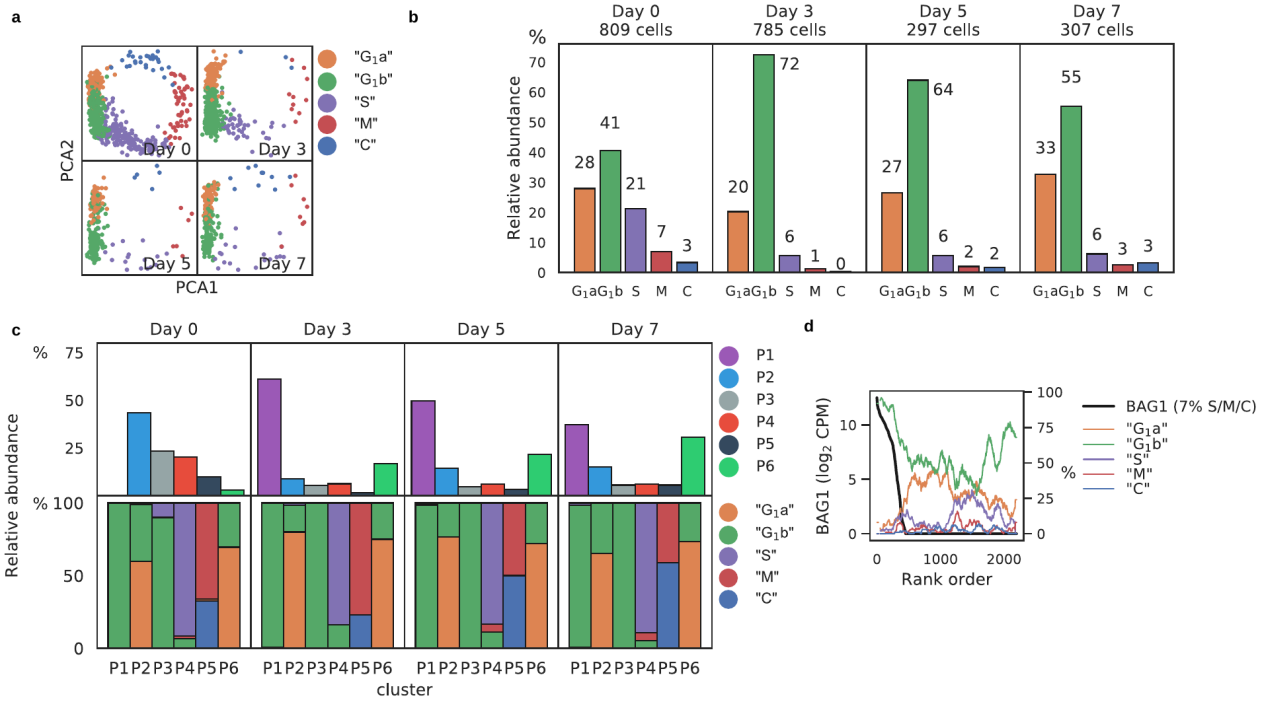

946

947**Figure 3 - Supplementary Figure 4. (a)** PCA projection of Pru stratified by days post induction (dpi) and 948colored by predicted cell cycle state. **(b)** Frequency of predicted cell cycle states at different dpi time 949points. **(c)** Frequency of Louvain clusters (top panels) and predicted cell cycle states in each cluster 950(bottom panels). **(d)** Rolling average frequency of predicted cell cycle states (colored lines) ordered by 951expression level of the canonical bradyzoite marker, *BAG1* (black line).

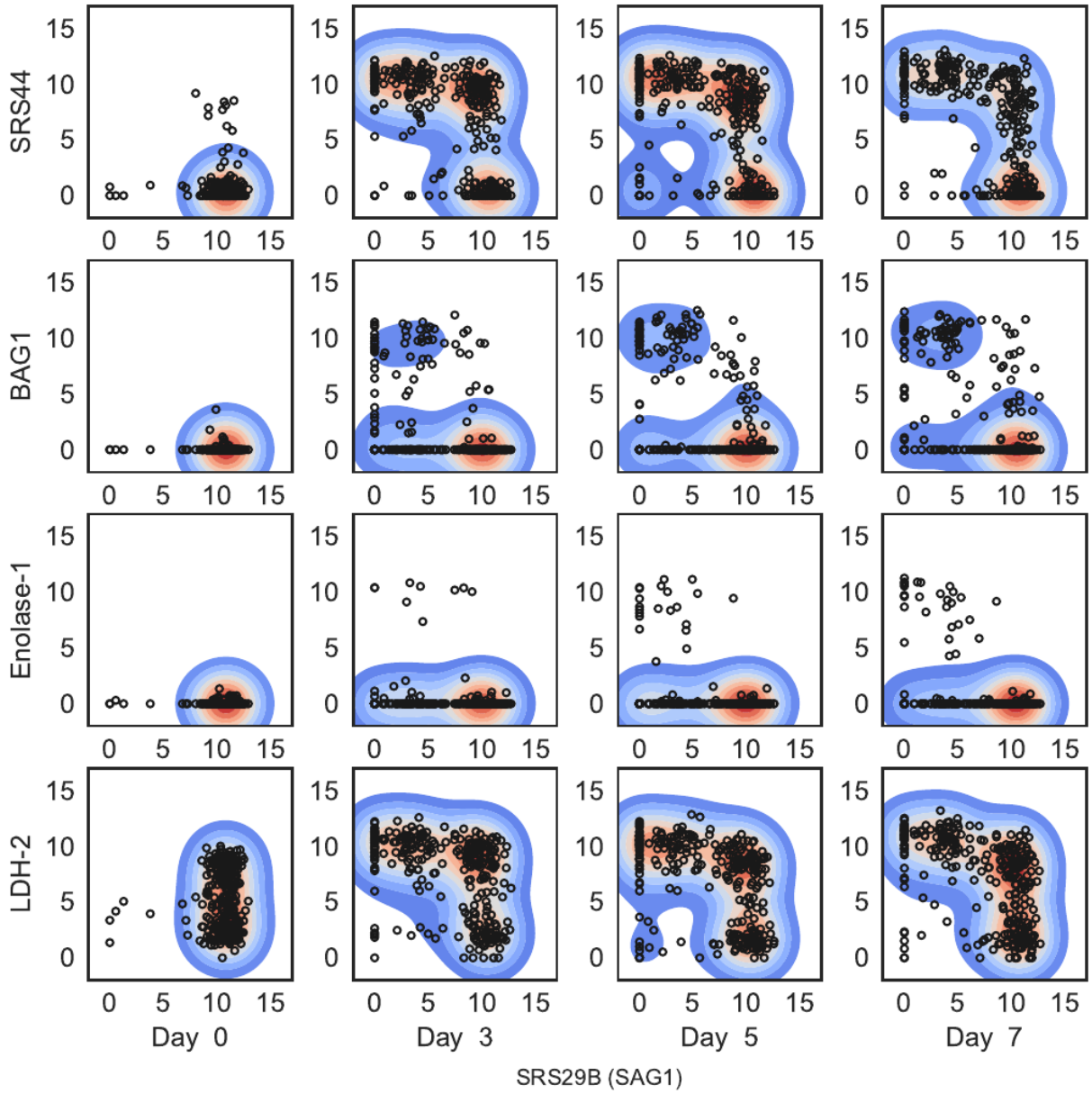

Figure 3 - Supplementary Figure 5. Expression level (log_2 CPM) of four "bradyzoite-specific" marker genes compared to that of "tachyzoite-specific" marker gene, *SAG1*, stratified by days post induction (dpi; columns).

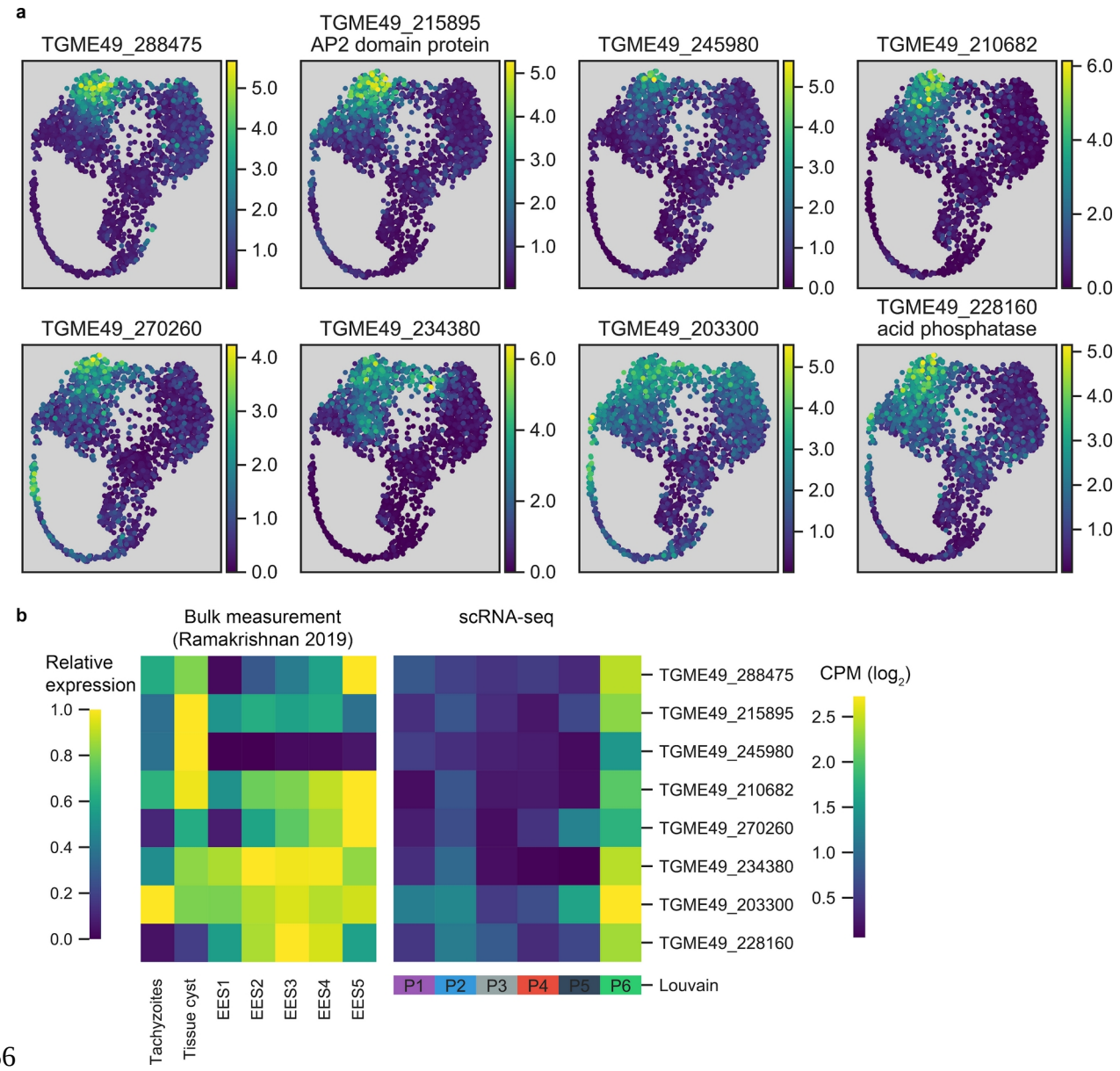

Figure 3 - Supplementary Figure 6. (a) UMAP projections of Pru colored by the neighbor-averaged expression ($\log_2$ CPM) of top 8 most differentially expressed and enriched genes in P6 cluster relative to P1 and P2, two most closely related clusters. **(b)** Comparison of P6-specific genes in bulk measurement of tachyzoites, tissue cysts, or enteroepithelial stages (EES1-EES5) (left) and scRNA-seq of Pru Louvain clusters (right).

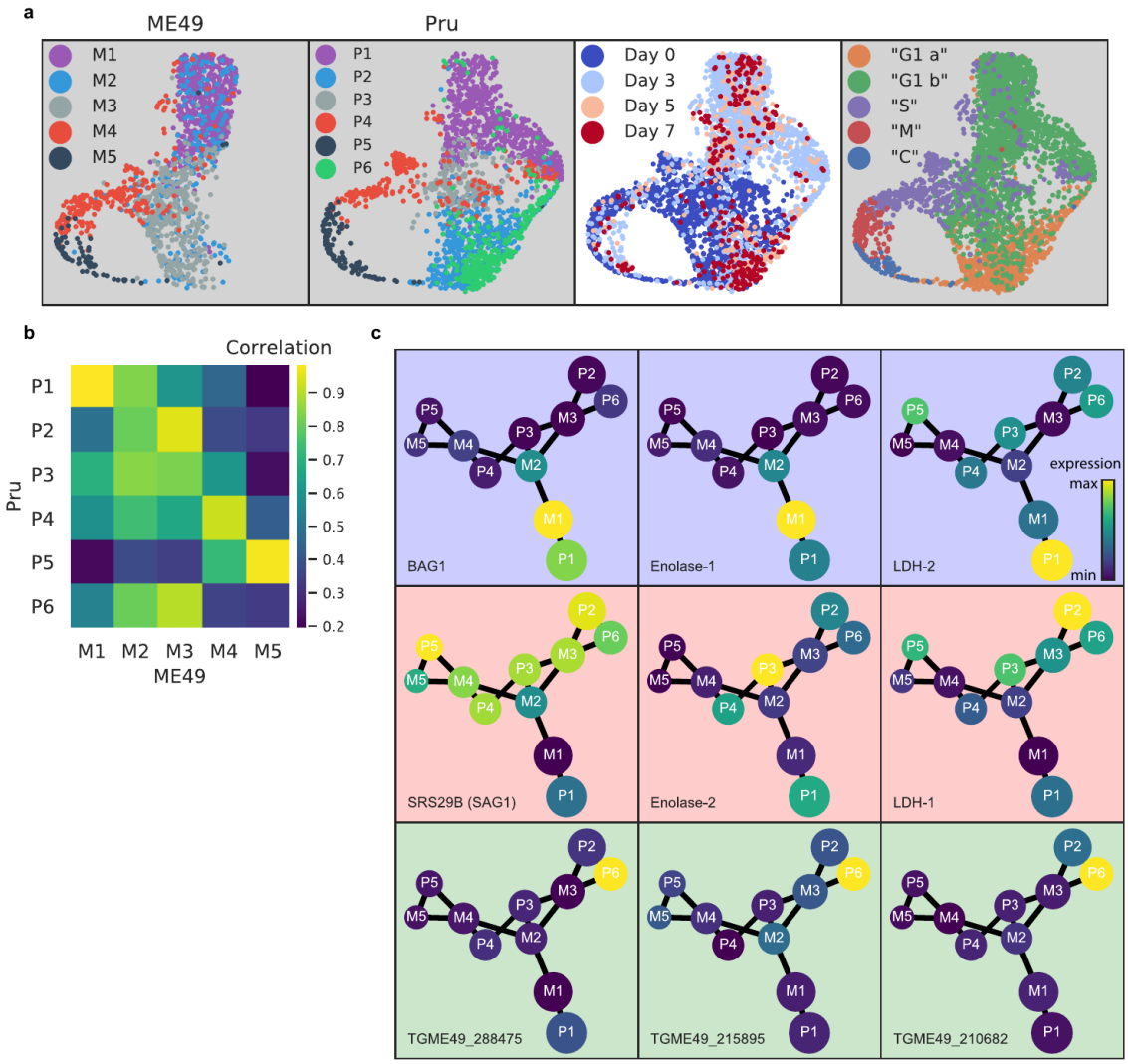

Figure 3 - Supplementary Figure 7. (a) UMAP projections of Pru and ME49 aligned by Scanorama. Cluster assignment was performed independently in each dataset. **(b)** Matrix correlation of cluster averaged expression between Pru and ME49. **(c)** Partition-based graph abstraction (PAGA) of aligned clusters with each being represented as a node connected by linkage with a connectivity threshold of 0.8. Node size reflects relative abundance of the cluster. Node colors reflect relative expression level of gene denoted in the bottom left of each panel, normalized to the maximum cluster expression of the corresponding data set (Pru or ME49). Three marker genes that are specific to bradyzoite (blue background), tachyzoite (red background), and Pru P6 cluster (green background) are shown.

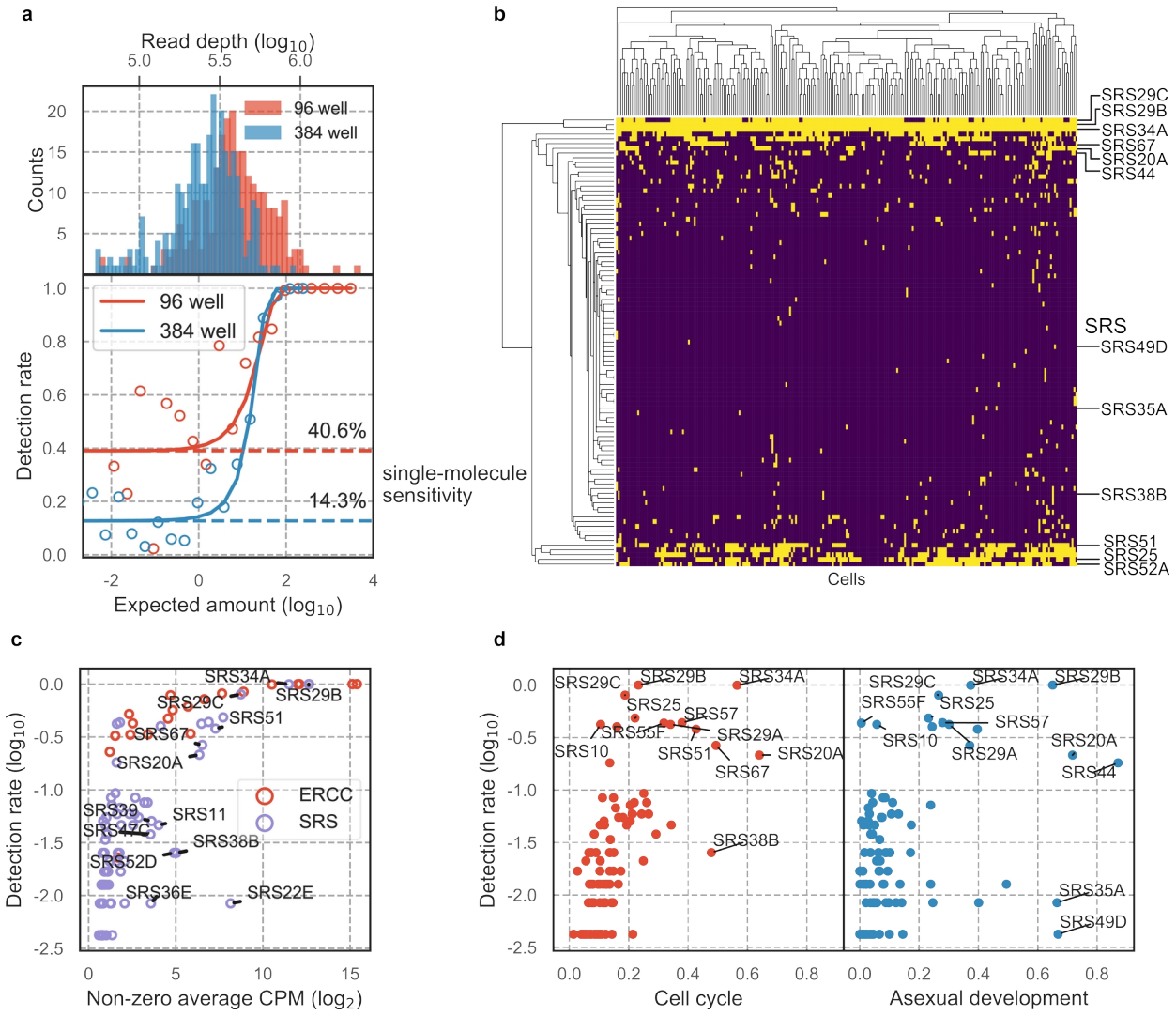

Figure 4. (a) Read depth (top) and detection rate of ERCC spike-ins (bottom) reveal higher measurement sensitvity in 96 well plate over 384 well plate format at roughly equivalent sequencing depth. **(b)** Hierarchical clustering heatmap of binarized expression reveals sparse expression pattern of SRS. SRS gene expression is binarized by converting expression $\geq$ 2 read counts to 1 and < 2 to 0. **(c)** Comparison of ERCCs with similar mean expression level reveals that low detection rate of SRS cannot be fully explained by measurement dropout. **(d)** We quantified the projection dependence score of SRS expression to cell cycle projection in 384-well RH or asexual development projection in 384-well Pru, reflecting the degree of co-variation of SRS expression with respect to these two biological processes. The detection rate in 96-well RH dataset is plotted along the y-axis. This analysis reveals that some of the SRS variation cannot be readily explained by either cell cycle or asexual development.

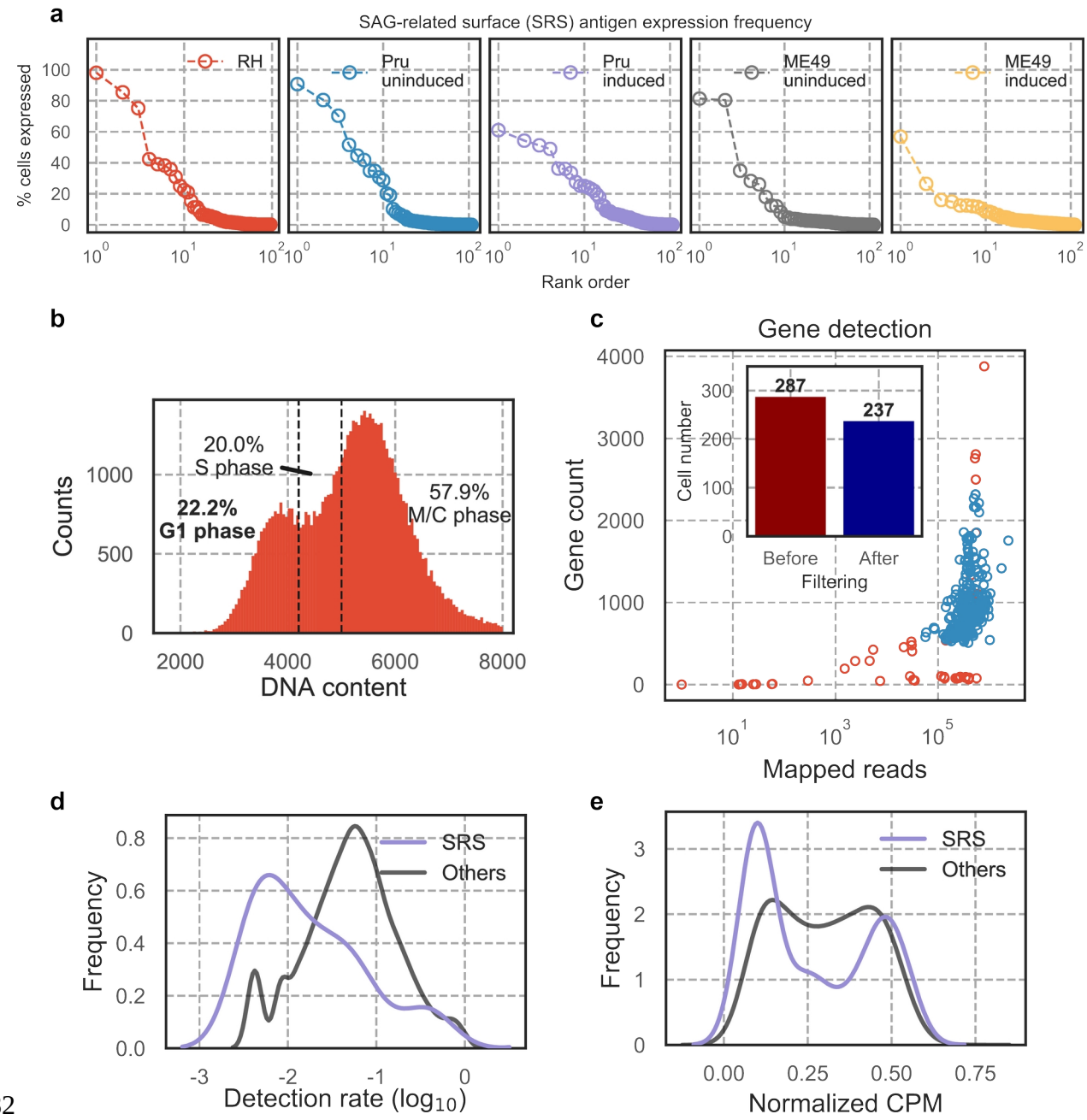

Figure 4 - Supplementary Figure 8. (a) *SRSs* rank ordered by percent expression in each single-parasite dataset. Each open circle depicts a single *SRS* in the corresponding dataset. **(b)** Fluorescence measurement of extracellular RH stained with DNA content stain. G1 sub-population was sorted into 96-well plate for scRNA-seq following Smart-seq 2 protocol. **(c)** Gene count (≥2 read counts) and read depth of 96-well scRNA-seq for cells that failed (red) or passed (blue) quality checking. Inset bar plot highlights the number of cells before and after filtering, revealing that ≥82% of cells passed quality checking. Majority of SRS is detected at lower frequency than most other *Toxoplasma* genes **(d)** and has low expression level **(e)**.

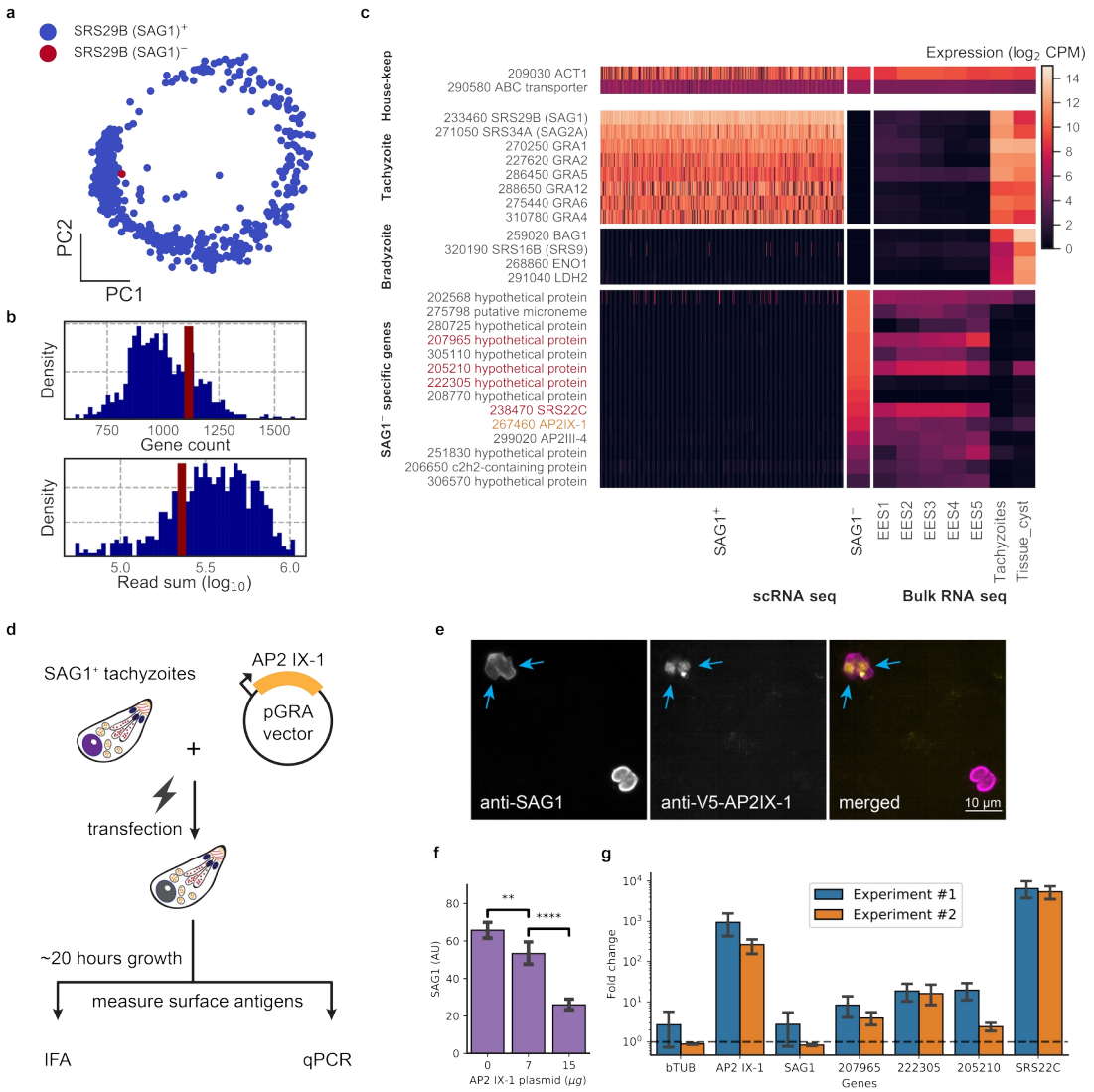

Figure 5. (a) PCA projection of 384-well RH cells colored by the presence (blue) or absence (red) of the SRS29B (SAG1) gene. **(b)** Gene count and total reads mapped for SAG1$^+$ (blue) and SAG1$^-$ (red) cells. **(c)** Comparison of house-keeping, tachyzoite-specific, bradyzoite-specific, and SAG1$^-$ enriched gene expression ($\log_2$ CPM) in scRNA-seq to bulk RNA-seq measurement of enteroepithelial stages (EES1-EES5), tachyzoites, and tissue cysts in RH. Genes that were pursued further by qRT-PCR are indicated in red; AP2IX-1 is colored orange. **(d)** Schematic illustration of transfection experiment. AP-2 IX-1 from genomic DNA of RH was cloned into a pGRA1 backbone vector and expressed constitutively in transfected parasites. Expression level of gene and protein was quantified with immunofluorescence assay (IFA) and qRT-PCR. **(e)** Representative IFA images showing anti-SAG1 (left), anti-V5-AP2IX-1 (center), and merged channels (right). Blue arrows point at parasites with detected expression of V5-AP2IX-1. **(f)** IFA quantification of anti-SAG1 signal shows dosage dependence of SAG1 protein expression on amount of AP2IX-1 plasmid transfected, with error bars depicting the standard deviation of quantification and asterisks representing statistical significance of two-tailed t-test for independence. **(g)** qPCR measurement shows that transfection of 15 µg AP2IX-1 plasmid, compared to no DNA control, induced the expression of AP2IX-1 and several putative surface antigens, including SRS22C, in two independent experiments with each measured in biological triplicates. AP2IX-1 transfection did not lead to increased expression of beta tubulin (bTUB) or SAG1. Error bars depict standard deviation of the measurement.

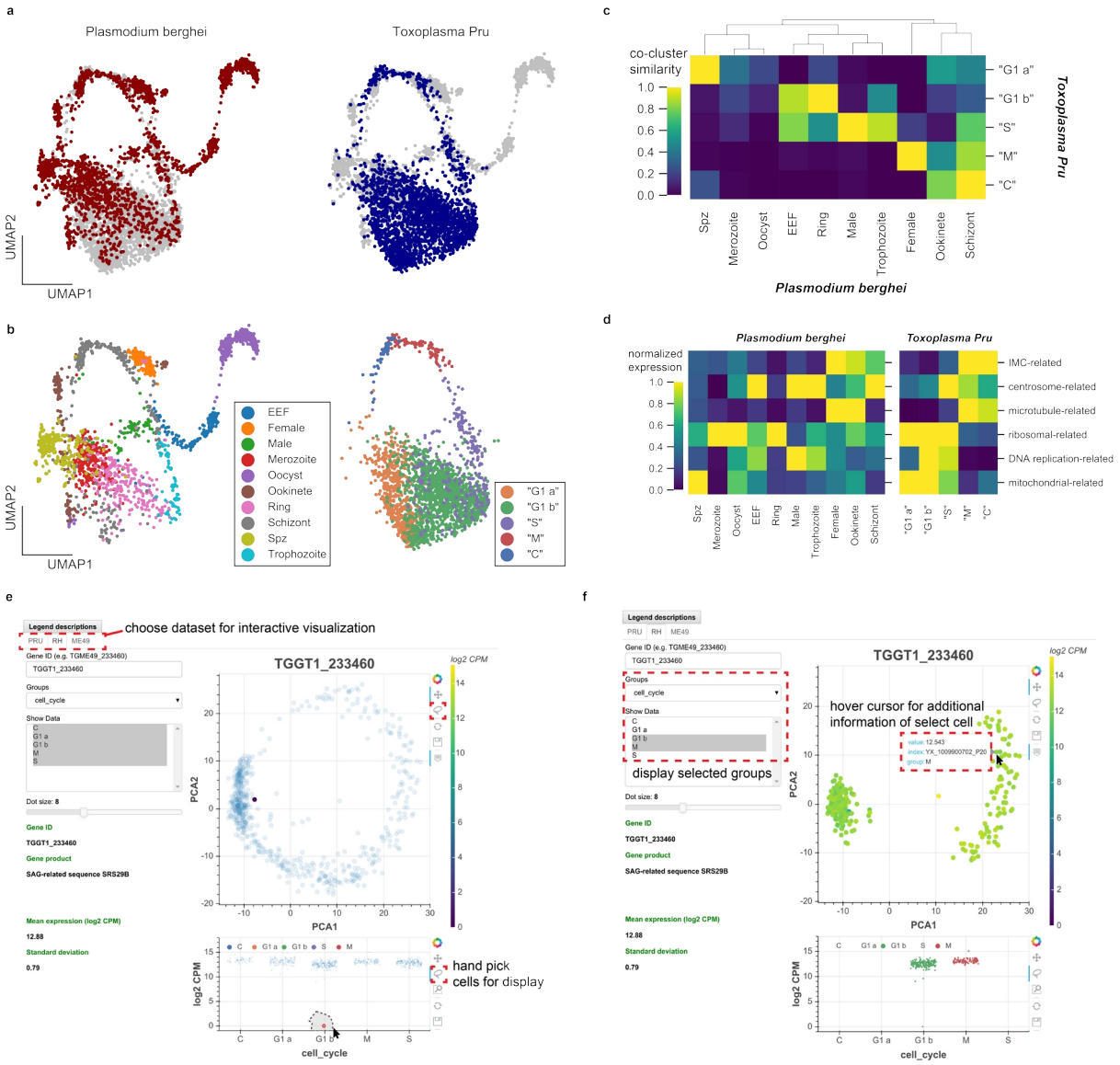

Figure 6. (a) Scanorama integration of *Plasmodium berghei* (red, left) and *Toxoplasma gondii* Pru (blue, right). **(b)** Cell cycle of *Toxoplasma* is well-aligned to the erythrocytic cycle of *Plasmodium berghei*, despite fundamental differences in cell cycle progression between these two apicomplexans. Each cell is colored by the original cluster assignment in the corresponding dataset. **(c)** Normalized cluster similarity between the original cluster assignment of *Plasmodium berghei* and *Toxoplasma Pru*. Cluster similarity is calculated by quantifying the fraction of cells that overlap in topological network in each cluster of the corresponding dataset. **(d)** Heatmap of concerted gene sets expression normalized to 1 within each cluster of cells in *Plasmodium* (left) and *Toxoplasma* (right). **(e)** Single-cell atlas of *Toxoplasma gondii* can be interactively visualized (http://st-atlas.org). Individual cells with distinct expression pattern can be highlighted using built-in graphical interface tools. **(f)** Groups of cells can be selectively displayed based on cell cycle state, developmental clusters, and other categories. Hovering over an individual cell with cursor reveals gene expression level, sample id, and group membership for further analysis. All our datasets are available for download on the atlas.

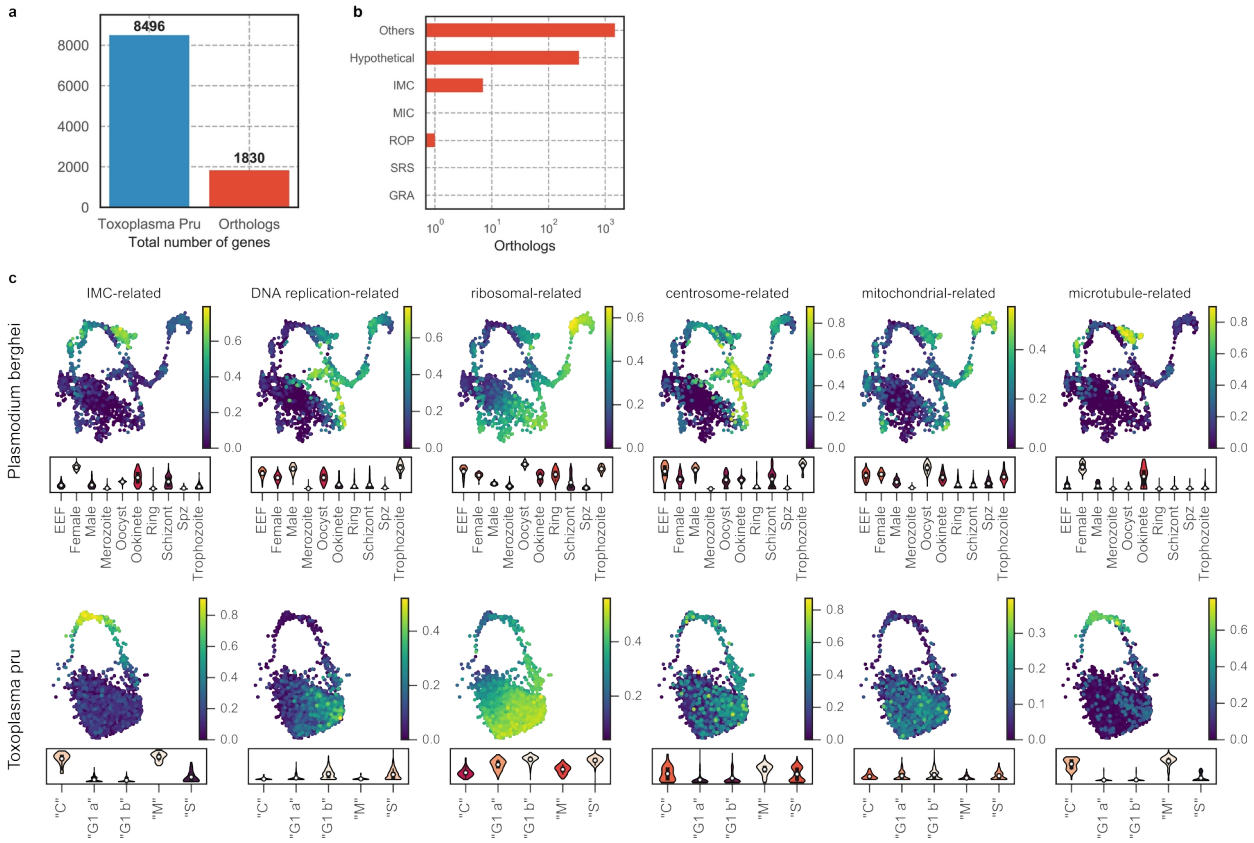

Figure 6 – Supplementary Figure 9. (a) Number of total *Toxoplasma* genes and one-to-one orthologs in *Plasmodium*. **(b)** Number of ortholog genes grouped by annotation in *Toxoplasma* genome. **(c)** UMAP projection of *Plasmodium berghei* **(top row)** or *Toxoplasma* Pru **(bottom row)** with cells colored by the average expression level of ortholog gene sets. The expression value is normalized to a maximum of 1 for each gene before taking the average such that the normalized value is not skewed towards genes with high dynamic range. Bottom panel of each subplot shows a violin plot of the average gene sets expression distribution stratified by cluster assignment. Gene sets covary in closely related regions of the projection space in both organisms.

Supplementary File 1. A list of sequence-based reagents (e.g. oligos) used in this study.

Supplementary File 2. A table of summary statistics and fold change of genes that are found to be differentially expressed between “G1 a” and “G1 b” parasites in RH. Genes are considered differentially expressed only if the adjusted p-values of Kruskal-Wallis test are less than 0.05 and that they are at least 2-fold over-expressed in either of the cell states.

Supplementary File 3. A table of summary statistics and fold change of genes that are found to be differentially expressed between across all cell cycle states in RH parasites. Genes are considered differentially expressed only if the adjusted p-values of Kruskal-Wallis test are less than 0.05 and that they are at least 2-fold over-expressed in any of the cell states.

Supplementary File 4. A table summarizing the hierarchical clustering results and encoded gene products. Clustering is performed on smoothened gene expression based on biological pseudotime in RH parasites.

Supplementary File 5. A table of summary statistics and fold change of genes that are found to be differentially expressed between across all clusters in Pru parasites. Genes are considered differentially expressed only if the adjusted p-values of Kruskal-Wallis test are less than 0.05.

Supplementary File 6. A table of summary statistics and fold change of genes that are found to be differentially expressed between across all clusters in ME49 parasites. Genes are considered differentially expressed only if the adjusted p-values of Kruskal-Wallis test are less than 0.05.

References

1. Pappas, G., Roussos, N. & Falagas, M. E. Toxoplasmosis snapshots: Global status of Toxoplasma gondii seroprevalence and implications for pregnancy and congenital toxoplasmosis. *Int. J. Parasitol.* (2009). doi:10.1016/j.ijpara.2009.04.003
2. Rabaud, C. *et al.* Extracerebral toxoplasmosis in patients infected with hiv a french national survey. *Med. (United States)* (1994). doi:10.1097/00005792-199411000-00004
3. Robert-Gangneux, F. *et al.* Molecular diagnosis of toxoplasmosis in immunocompromised patients: A 3-year multicenter retrospective study. *J. Clin. Microbiol.* (2015). doi:10.1128/JCM.03282-14
4. Sutterland, A. L. *et al.* Beyond the association. Toxoplasma gondii in schizophrenia, bipolar disorder, and addiction: Systematic review and meta-analysis. *Acta Psychiatr. Scand.* (2015). doi:10.1111/acps.12423
5. Vyas, A., Kim, S.-K., Giacomini, N., Boothroyd, J. C. & Sapolsky, R. M. Behavioral changes induced by Toxoplasma infection of rodents are highly specific to aversion of cat odors. *Proc. Natl. Acad. Sci.* (2007). doi:10.1073/pnas.0608310104
6. Soête, M., Camus, D. & Dubrametz, J. F. Experimental induction of bradyzoite-specific antigen expression and cyst formation by the RH strain of Toxoplasma gondii in vitro. *Exp. Parasitol.* (1994). doi:10.1006/expr.1994.1039
7. Jeffers, V., Tampaki, Z., Kim, K. & Sullivan, W. J. A latent ability to persist: differentiation in Toxoplasma gondii. *Cellular and Molecular Life Sciences* (2018). doi:10.1007/s00018-018-2808-x
8. Buchholz, K. R. *et al.* Identification of Tissue Cyst Wall Components by Transcriptome Analysis of In Vivo and In Vitro Toxoplasma gondii Bradyzoites . *Eukaryot. Cell* (2011). doi:10.1128/ec.05182-11
9. Manger, I. D. *et al.* Expressed Sequence Tag Analysis of the Bradyzoite Stage of Toxoplasma gondii: Identification of Developmentally Regulated Genes. *Infect. Immun.* (1998).
10. Pittman, K. J., Aliota, M. T. & Knoll, L. J. Dual transcriptional profiling of mice and Toxoplasma gondii during acute and chronic infection. *BMC Genomics* (2014). doi:10.1186/1471-2164-15-806
11. Yip, K. Our implementation of the SCA method. 1–4 (2007).
12. Cleary, M. D., Singh, U., Blader, I. J., Brewer, J. L. & Boothroyd, J. C. Toxoplasma gondii Asexual Development: Identification of Developmentally Regulated Genes and Distinct Patterns of Gene Expression . *Eukaryot. Cell* (2002). doi:10.1128/ec.1.3.329-340.2002
13. Radke, J. R. *et al.* The transcriptome of Toxoplasma gondii. *BMC Biology* (2005). doi:10.1186/1741-7007-3-26
14. Chen, L. F. *et al.* Comparative studies of Toxoplasma gondii transcriptomes: Insights into stage conversion based on gene expression profiling and alternative splicing. *Parasites and Vectors* (2018). doi:10.1186/s13071-018-2983-5
15. Fouts, A. E. & Boothroyd, J. C. Infection with Toxoplasma gondii bradyzoites has a diminished impact on host transcript levels relative to tachyzoite infection. *Infect. Immun.* (2007). doi:10.1128/IAI.01228-06
16. Hong, D.-P., Radke, J. B. & White, M. W. Opposing Transcriptional Mechanisms Regulate Toxoplasma Development . *mSphere* (2017). doi:10.1128/msphere.00347-16
17. White, M. W., Radke, J. R. & Radke, J. B. Toxoplasma development - turn the switch on or off? *Cellular Microbiology* (2014). doi:10.1111/cmi.12267
18. Soete, M., Fortier, B., Camus, D. & Dubremetz, J. F. Toxoplasma gondii: Kinetics of bradyzoite-tachyzoite interconversion in vitro. *Exp. Parasitol.* (1993). doi:10.1006/expr.1993.1031

10. Watts, E. *et al.* Novel Approaches Reveal that Toxoplasma gondii Bradyzoites within Tissue Cysts Are Dynamic and Replicating Entities In Vivo. *MBio* (2015). doi:10.1128/mbio.01155-15
20. Ferguson, D. J. P., Huskinson-Mark, J., Araujo, F. G. & Remington, J. S. A morphological study of chronic cerebral toxoplasmosis in mice: comparison of four different strains of Toxoplasma gondii. *Parasitol. Res.* (1994). doi:10.1007/BF00932696
21. Radke, J. R., Guerini, M. N., Jerome, M. & White, M. W. A change in the premitotic period of the cell cycle is associated with bradyzoite differentiation in Toxoplasma gondii. *Mol. Biochem. Parasitol.* (2003).
22. Sinai, A. P. *et al.* Reexamining Chronic Toxoplasma gondii Infection: Surprising Activity for a “Dormant” Parasite. *Current Clinical Microbiology Reports* (2016). doi:10.1007/s40588-016-0045-3
23. Jerome, M. E., Radke, J. R., Bohne, W., Roos, D. S. & White, M. W. Toxoplasma gondii bradyzoites form spontaneously during sporozoite- initiated development. *Infect. Immun.* (1998).
24. Ali, F. *et al.* Cell cycle-regulated multi-site phosphorylation of Neurogenin 2 coordinates cell cycling with differentiation during neurogenesis. *Development* (2011). doi:10.1242/dev.067900
25. Kim, D. H. *et al.* The CRL4Cdt2 Ubiquitin Ligase Mediates the Proteolysis of Cyclin-Dependent Kinase Inhibitor Xic1 through a Direct Association with PCNA. *Mol. Cell. Biol.* (2010). doi:10.1128/mcb.01135-09
26. Radke, J. R. & White, M. W. A cell cycle model for the tachyzoite of Toxoplasma gondii using the Herpes simplex virus thymidine kinase. *Mol. Biochem. Parasitol.* (1998). doi:10.1016/S0166-6851(98)00074-7
27. Conde de Felipe, M. M., Lehmann, M. M., Jerome, M. E. & White, M. W. Inhibition of Toxoplasma gondii growth by pyrrolidine dithiocarbamate is cell cycle specific and leads to population synchronization. *Mol. Biochem. Parasitol.* (2008). doi:10.1016/j.molbiopara.2007.09.003
28. Behnke, M. S. *et al.* Coordinated progression through two subtranscriptomes underlies the tachyzoite cycle of toxoplasma gondii. *PLoS One* (2010). doi:10.1371/journal.pone.0012354
29. Wang, B. *et al.* Stem cell heterogeneity drives the parasitic life cycle of Schistosoma mansoni. 1–23 (2018).
30. Reid, A. J. *et al.* Single-cell RNA-seq reveals hidden transcriptional variation in malaria parasites. *Elife* **7**, 1–29 (2018).
31. Ngara, M. *et al.* Exploring parasite heterogeneity using single-cell RNA-seq reveals a gene signature among sexual stage Plasmodium falciparum parasites. *Exp. Cell Res.* (2018). doi:10.1016/j.yexcr.2018.08.003
32. Poran, A. *et al.* Single-cell RNA sequencing reveals a signature of sexual commitment in malaria parasites. *Nature* **551**, 95–99 (2017).
33. Howick, V. M. *et al.* The Malaria Cell Atlas: Single parasite transcriptomes across the complete Plasmodium life cycle . *Science (80-.).* **365**, eaaw2619 (2019).
34. Svensson, V. *et al.* Power analysis of single-cell RNA-sequencing experiments. *Nat. Methods* **14**, 381–387 (2017).
35. Ziegenhain, C. *et al.* Comparative Analysis of Single-Cell RNA Sequencing Methods. *Mol. Cell* (2017). doi:10.1016/j.molcel.2017.01.023
36. Reid, A. J. Large, rapidly evolving gene families are at the forefront of host-parasite interactions in Apicomplexa. *Parasitology* (2014). doi:10.1017/S0031182014001528
37. Lönnberg, T. *et al.* Single-cell RNA-seq and computational analysis using temporal mixture modeling resolves T_H1/T_{FH} fate bifurcation in malaria. *Sci. Immunol.* **2**, eaal2192 (2017).

Ziegenhain, C. *et al.* Comparative Analysis of Single-Cell RNA Sequencing Methods. *Mol. Cell* **65**, 631-643.e4 (2017).

La Manno, G. *et al.* RNA velocity of single cells. *Nature* (2018). doi:10.1038/s41586-018-0414-6

Wolf, F. A., Angerer, P. & Theis, F. J. SCANPY: large-scale single-cell gene expression data analysis. *Genome Biol.* (2018). doi:10.1186/s13059-017-1382-0

Gajria, B. *et al.* ToxoDB: An integrated toxoplasma gondii database resource. *Nucleic Acids Res.* **36**, 553–556 (2008).

Beraki, T. *et al.* Divergent kinase regulates membrane ultrastructure of the Toxoplasma parasitophorous vacuole . *Proc. Natl. Acad. Sci.* (2019). doi:10.1073/pnas.1816161116

Camejo, A. *et al.* Identification of three novel Toxoplasma gondii rhoptry proteins. *Int. J. Parasitol.* (2014). doi:10.1016/j.ijpara.2013.08.002

Beck, J. R. *et al.* A Toxoplasma Palmitoyl Acyl Transferase and the Palmitoylated Armadillo Repeat Protein TgARO Govern Apical Rhoptry Tethering and Reveal a Critical Role for the Rhoptries in Host Cell Invasion but Not Egress. *PLoS Pathog.* **9**, (2013).

Coffey, M. J. *et al.* Aspartyl Protease 5 Matures Dense Granule Proteins That Reside at the Host-Parasite Interface in Toxoplasma gondii . *MBio* (2018). doi:10.1128/mbio.01796-18

Jones, N. G., Wang, Q. & Sibley, L. D. Secreted protein kinases regulate cyst burden during chronic toxoplasmosis. *Cell. Microbiol.* (2017). doi:10.1111/cmi.12651

McInnes, L., Healy, J., Saul, N. & Großberger, L. UMAP: Uniform Manifold Approximation and Projection. *J. Open Source Softw.* (2018). doi:10.21105/joss.00861

De Silva, E. K. *et al.* Specific DNA-binding by Apicomplexan AP2 transcription factors. *Proc. Natl. Acad. Sci. U. S. A.* **105**, 8393–8398 (2008).

Radke, J. B. *et al.* ApiAP2 transcription factor restricts development of the Toxoplasma tissue cyst. *Proc. Natl. Acad. Sci. U. S. A.* **110**, 6871–6876 (2013).

Walker, R. *et al.* Toxoplasma transcription factor TgAP2XI-5 regulates the expression of genes involved in parasite virulence and host invasion. *J. Biol. Chem.* **288**, 31127–31138 (2013).

Ramakrishnan, C. *et al.* An experimental genetically attenuated live vaccine to prevent transmission of Toxoplasma gondii by cats. *Sci. Rep.* (2019). doi:10.1038/s41598-018-37671-8

Hie, B., Bryson, B. & Berger, B. Efficient integration of heterogeneous single-cell transcriptomes using Scanorama. *Nat. Biotechnol.* **37**, 685–691 (2019).

Wolf, F. A. *et al.* PAGA: graph abstraction reconciles clustering with trajectory inference through a topology preserving map of single cells. *Genome Biol.* (2019). doi:10.1186/s13059-019-1663-x

Manger, I. D., Hehl, A. B. & Boothroyd, J. C. The surface of Toxoplasma tachyzoites is dominated by a family of glycosylphosphatidylinositol-anchored antigens related to SAG1. *Infect. Immun.* **66**, 2237–2244 (1998).

Kim, S.-K. & Boothroyd, J. C. Stage-Specific Expression of Surface Antigens by Toxoplasma gondii as a Mechanism to Facilitate Parasite Persistence. *J. Immunol.* (2005). doi:10.4049/jimmunol.174.12.8038

Kim, S. K., Karasov, A. & Boothroyd, J. C. Bradyzoite-specific surface antigen SRS9 plays a role in maintaining Toxoplasma gondii persistence in the brain and in host control of parasite replication in the intestine. *Infect. Immun.* **75**, 1626–1634 (2007).

Zanto, T. P., Hennigan, K., Östberg, M., Clapp, W. C. & Gazzaley, A. Malaria Parasite Development in the Mosquito and Infection of the Mammalian Host. *Annu. Rev. Microbiol.* **46**, 564–574 (2011).

Cowman, A. F., Healer, J., Marapana, D. & Marsh, K. Malaria: Biology and Disease. *Cell* **167**, 610–624 (2016).

Hie, B. L., Bryson, B. & Berger, B. Panoramic stitching of heterogeneous single-cell transcriptomic data. *bioRxiv* (2018). doi:10.1101/371179

Weiss, L. M., Ma, Y. F., Takvorian, P. M., Tanowitz, H. B. & Wittner, M. Bradyzoite development in Toxoplasma gondii and the hsp70 stress response. *Infect. Immun.* (1998).

Litzenburger, U. M. *et al.* Single-cell epigenomic variability reveals functional cancer heterogeneity. *Genome Biol.* **18**, 1–12 (2017).

Elowitz, M. B., Levine, A. J., Siggia, E. D. & Swain, P. S. Stochastic gene expression in a single cell. *Science (80-.).* **297**, 1183–1186 (2002).

Butler, A., Hoffman, P., Smiberg, P., Papalexi, E. & Satija, R. Integrating single-cell transcriptomic data across different conditions, technologies, and species. *Physiol. Behav.* **176**, 139–148 (2017).

Ding, H., Blair, A., Yang, Y. & Stuart, J. M. Biological process activity transformation of single cell gene expression for cross-species alignment. *Nat. Commun.* **10**, 4899 (2019).

WEISS, L. M. *et al.* A Cell Culture System for Study of the Development of Toxoplasma gondii Bradyzoites. *J. Eukaryot. Microbiol.* (1995). doi:10.1111/j.1550-7408.1995.tb01556.x

Picelli, S. *et al.* Full-length RNA-seq from single cells using Smart-seq2. *Nat. Protoc.* (2014). doi:10.1038/nprot.2014.006

Panas, M. W., Naor, A., Cygan, A. M. & Boothroyd, J. C. *Toxoplasma controls host cyclin E expression through the use of a novel myr1-dependent effector protein, HCE1*. *mBio* **10**, (2019).

Livak, K. J. & Schmittgen, T. D. Analysis of relative gene expression data using real-time quantitative PCR and the 2-ΔΔCT method. *Methods* **25**, 402–408 (2001).

Tarashansky, A. J., Xue, Y., Li, P., Quake, S. R. & Wang, B. Self-assembling manifolds in single-cell RNA sequencing data. *Elife* **8**, 1–29 (2019).

Traag, V. A., Waltman, L. & van Eck, N. J. From Louvain to Leiden: guaranteeing well-connected communities. *Sci. Rep.* **9**, 1–12 (2019).